Unlocking the potential of Triaxus for studying biogeochemistry

By

Hongkun Zhang

Bachelor of Marine and Antarctic Science with Honours

University of Tasmania, July 2019

Supervisors: Zanna Chase, Christina Schallenberg and Helen Phillips

A thesis submitted in partial fulfilment of the requirements of the Bachelor of Marine and Antarctic Science with Honours at the Institute for Marine and Antarctic Studies (IMAS), University of Tasmania, June 2020

Declaration:

I declare that this thesis contains no material which has been accepted for the award of any other degree or diploma in any tertiary institution, and that, to the best of the my knowledge and belief, this thesis contains no material previously published or written by another person, except where due reference is made in the text of this thesis.

Hongkun Zhang

21st June, 2019

Abstract

This study explores the potential of Triaxus data for understanding biogeochemical processes, particularly in the East Australian Current (EAC). Triaxus is a towed undulating apparatus which has been used on *RV Investigator* (a marine research vessel from CSIRO) for several years. There are 15 available Triaxus datasets collected by *RV Investigator*. This study initially evaluated the quantity and quality of these datasets. Additionally, the fine-scale vertical resolution and spatial coverage of Triaxus data can provide a special perspective on biogeochemical processes, which is distinct from that seen with traditional measurements such as ship-based vertical CTD profiles, profiling floats and satellite remote sensing. However, up to now, the potential of Triaxus data has barely been explored, particularly for biogeochemical work.

In this study, we found 4 tows that revealed very interesting features that we identified as suspected subduction events, which could carry carbon into the ocean interior and impact the carbon cycle in the ocean. We combined ship-based measurements (primarily Triaxus) and satellite measurements to investigate the likely mechanism (subduction or gravitational sinking) associated with eddies and fronts of this feature and other similar features found in other voyages. It was found that the occurrence of subduction events was closely related to the horizontal and vertical motions of surrounding water associated with eddies and fronts, with phenomena of high dissolved oxygen (DO), low apparent oxygen utilization (AOU) and weak stratification, while the occurrence of sinking due to gravity was accompanied by observations of low DO, high AOU, well-structured water masses and strong stratification.

Acknowledgements

This thesis embodies all my harvest in this honour year, and also contains much help of most people. I would like to thank all of you for helping me in writing this thesis.

My deepest gratitude is first to my honorific supervisors: Zanna Chase, Christina Schallenberg and Helen Phillips for their constant encouragement, guidance and assistance, allowing me to constantly explore new knowledge and improve my academic ability. Without their enlightening and patient guidance, I would not have completed my research, and this paper would not have been in its present form. I would also like to thank them for taking so much time to hold so many meetings with me. Do not mind my poor oral English and patiently answer all questions I have in my project work. I would also like to thank them very much for taking so much time to comment my drafts and correct my mistakes. At the same time, I am also very grateful to them for their care, encouragement and support when I suffer setbacks.

Secondly, I would also like to express my heartfelt gratitude to the proof-reader, Scott Hadley, for his comments on this thesis. In particular, his corrections of English grammar and vocabulary make this thesis more comfortable to read.

Thirdly, I would like to thank all the staff and researchers from IMAS and CSIRO for the data and help.

Finally, I would like to express my sincere thanks to my family for their love and care in me. I would also like to thank my friends who helped me in the difficult process of my project.

List of figures: Figure (Fig .)

List of tables

Contents

1. Introduction

1.1 The Triaxus, its biogeochemical sensors and working principle

Triaxus is a towed oceanographic platform that has been used for many years in marine science primarily for sound velocity profile measurements and CTD applications (Hansen & Hansen 2003). It has been used since 2014 on the *RV Investigator* (a marine research vessel belongs to the Commonwealth Scientific and Industrial Research Organisation **(**CSIRO)) to investigate oceanographic regions around Australia, such as the East Australian Current and Southern Ocean. The vehicle is designed to be towed up to 3 km behind a ship and undulates between the surface and ~ 200-350 metres depth. By controlling its fight path scientists onboard the *RV Investigator* can create a two-dimensional image of the upper ocean. The apparatus is capable of taking high resolution profiles due to a relatively high vertical speed ($1ms^{-1}$) in relation to the towing speed (2-10 knots).

Many typical oceanographic sensors are deployed on Triaxus, including sensors that measure temperature, salinity and pressure. Parameters of biogeochemical relevance, including dissolved oxygen, chlorophyll fluorescence, backscatter, coloured dissolved organic matter (CDOM) and transmissivity of seawater can also be measured. Furthermore, Triaxus can also be fitted with more sophisticated and user-supplied sensors to measure photosynthetic performance, *in situ* concentration of nitrate and distribution of plankton in seawater. All of the above parameters collected by Triaxus can be transferred to the ship by a fibre optic cable in real-time.

Many of the typical sensors mentioned above are relevant to studying biogeochemistry of the ocean. The sensor deployed on the Triaxus platform to measure temperature, salinity and pressure is known as a CTD (conductivity, temperature and depth). The dominant function of the CTD is to detect how conductivity and temperature change with depth in a water column. Conductivity can be combined with temperature and

pressure to derive the corresponding ocean salinity at the same depth. A Sea-Bird SBE43 sensor is used to measure dissolved oxygen. It is a Clark polarographic membrane sensor that measures the concentration of dissolved oxygen in a water column by detecting the oxygen molecules entering the sensing foil on the sensing window (Martini, Butman & Mickelson 2007). The ECO Triplet deployed on the Triaxus platform is a backscattering and fluorescence sensor equipped with three optical sensors to respectively measure chlorophyll and CDOM fluorescence and red backscattering. The fluorescence sensor can provide excitation at one wavelength and measures the corresponding fluorescence including chlorophyll and CDOM. The backscatter sensor emits light in the red wavelengths and detects backscattered light from suspended particles and seawater. Optical measurements of chlorophyll fluorescence and backscatter can be used to estimate concentrations of chlorophyll-a and particulate organic carbon (POC) (Johnson et al. 2017). Under certain conditions, e.g. in the open ocean, the concentration of POC can be closely correlated to the value of particulate optical backscattering (b_{bp}) estimated by the backscatter sensor (Briggs et al. 2011; Cetinić et al. 2012). Dissolved organic matter (DOM) represents all dissolved organic matter in a water column, including organic molecules released by various organisms. The type and amount of DOM are based on the proportion of light which is absorbed in a particular wavelength and then released at a longer wavelength (Bushnell, Kinkade & Worthington 2017). Furthermore, the optically measurable component of DOM is called CDOM which can also fluoresce (Bushnell, Kinkade & Worthington 2017) and then can be detected with a fluorescence sensor as we have on the Triaxus, which allows researchers to quantify the abundance of dissolved organic matter in a water sample by using fluorometry. The transmissometer can estimate the transmissivity of light in the water, which can be used to evaluate the concentration of suspended or particulate matter in seawater (Thomson & Emery 2014). Overall, these typical sensors deployed on the Triaxus platform can provide extensive biogeochemical information, which is the motivation for this study.

In addition, there are more sophisticated and user-supplied sensors that can be deployed on Triaxus. These include a photosynthetically available radiation sensor, a nitrate sensor and a laser optical plankton counter (LOPC) sensor. PAR (photosynthetic active radiation) is the solar energy available for photosynthesis. The PAR sensor can be used to measure photosynthetic light levels in both air and water. The spectral range of PAR is defined as 400-700 nanometre as these wavelengths are relevant for photosynthesis (Frouin & Murakami 2007). The nitrate sensor is widely used in two types: ISUS (In Situ Ultraviolet Spectrophotometer) and SUNA (Submersible Ultraviolet Nitrate Analyzer). Both the ISUS and SUNA are optical sensors, which can measure *in situ* concentrations directly by utilizing the UV absorption characteristics of dissolved nitrate without the need of reagents, thus providing reliable nitrate measurements from distant and unmanned platforms (Johnson & Coletti 2002). The LOPC sensor can measure the cross-sectional area of passing particles with its laser beam to collect real-time information about the dimension and abundance of particles, which can reflect the distribution of plankton in seawater (Schultes & Lopes 2009).

1.2 Ocean eddies and fronts

Ocean eddies are vortexes in the ocean ranging in diameter from centimetres to hundreds of kilometres and are generated by the geostrophic instability (Vallis 2006). Eddies are divided into two types, cyclonic eddies and anti-cyclonic eddies (Fig 1). Cyclonic eddies are cold-core with a lower sea surface at the centre than the surrounding water due to the upwelling from the thermocline, where horizontal fluid near the sea surface flows from the centre to the edge (Fig 1a; Bakun 2006); Anti-cyclonic eddies are warm-core with the higher sea surface at the centre than the surrounding water due to the downwelling from sea surface with smaller density, and horizontal fluid near the sea surface flows from the edge to the centre of eddies (Fig 1b; Bakun 2006). The most common ocean eddies are mesoscale eddies, with a diameter

of 100-200 km, which are found ubiquitously in the global ocean. They increase the rate at which water masses migrate from the ocean surface to the interior thermocline, especially in areas of intense baroclinic instability, such as strong currents like the Antarctic Circumpolar Current and ocean fronts (Marshall 1997).

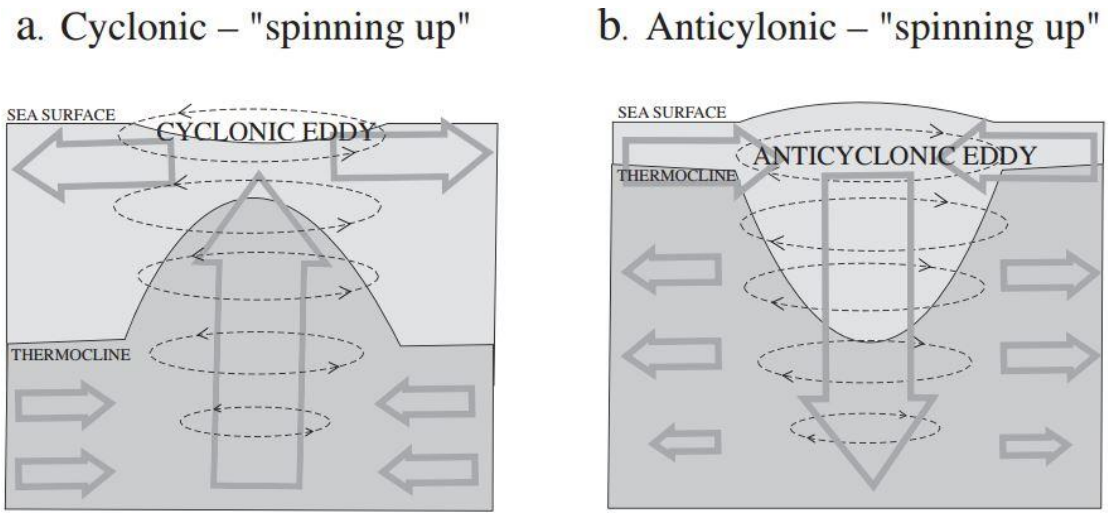

Figure 1. Schematic of (a) a cyclonic eddy and (b) an anti-cyclonic eddy (Bakun 2006). The arrows indicate the direction of flow underwater.

Ocean fronts are the interface between two water masses with diverse physical characteristics. These generally present as intense horizontal gradients of temperature and salinity, leading to a variation in density and current shear (Fig 2). Near the fronts, a water mass with intermediate density, generated by the mixing of two water masses with differing densities near the interface, flows downward below the less dense surface water, carrying with particles from the surface layer (Fig 2; Bakun 2006). The spatial distribution of ocean fronts presents a structure of narrow filaments (Sokolov & Rintoul 2002), where the transfer of ocean energy from large scales to small scales is the most intense (Rubenstein & Roberts 1986). Ocean fronts are closely linked to mesoscale eddies. Eddies at this scale can create fronts and conversely the baroclinic and barotropic instability of a front can produce these features (Badin et al. 2009). Additionally, both eddies and fronts have been shown to facilitate organic carbon export to the deep ocean (Honjo et al. 1999; Stukel et al. 2017; Sweeney 2001), which is related

to the air-sea exchange of carbon.

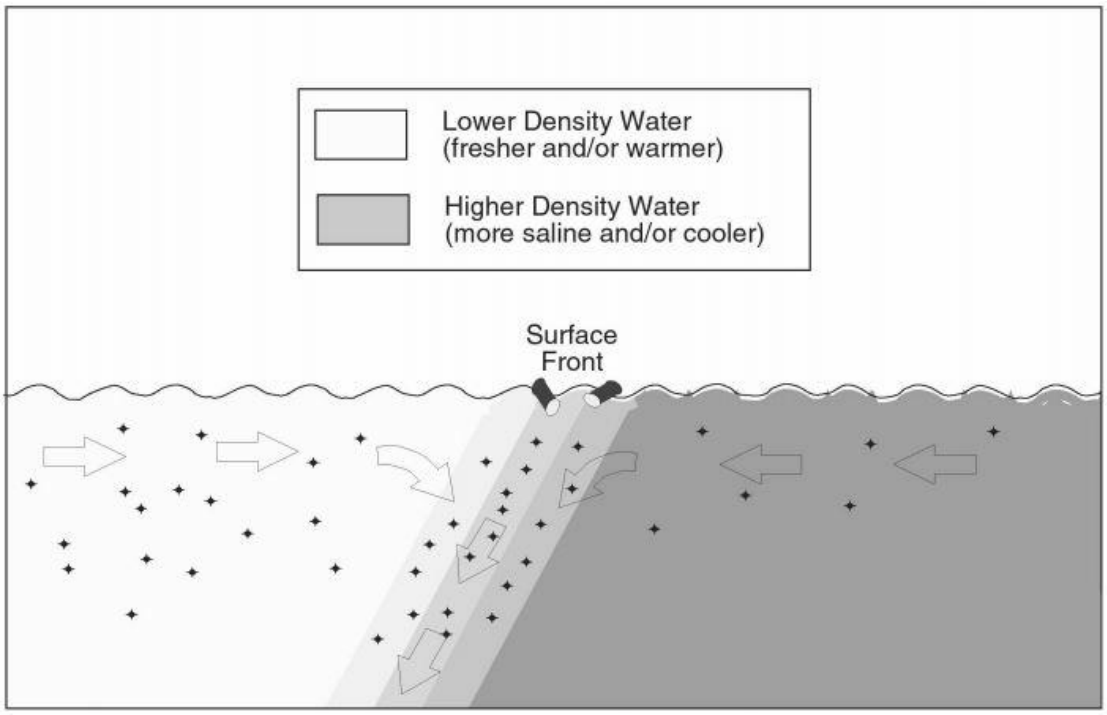

Figure 2. Schematic diagram of a front between water mass with different density or temperature (Bakun 2006). The arrows indicate the direction of flow underwater. The black stars represent particles in the upper ocean.

1.3 Ocean biological carbon pump

The ocean biological carbon pump plays an important role in the sea-air exchange of carbon, which is an essential component of the global carbon cycle. It refers to the process whereby phytoplankton on the sea surface, where sunlight is sufficient, converts dissolved inorganic carbon into organic carbon through photosynthesis (Fig 3). Most of the organic carbon is then converted back into carbon dioxide through consumption by zooplankton and bacteria in the upper layer (Neuer, Iversen & Fischer 2014). However, a small amount of organic carbon produced in the upper ocean can be transported directly to the deeper interior through physical deposition. This pump sequesters carbon dioxide for weeks to hundreds of years or even millions of years on a geologic timescale (Neuer, Iversen & Fischer 2014), and plays a vital role in the distribution of carbon dioxide between the atmosphere and ocean (McGillicuddy et al.

2007). As mentioned previously, a small amount of organic carbon is exported by physical deposition. This is achieved through two main processes: gravitational sinking and subduction. Gravitational sinking is generally regarded as the predominant process behind vertical transport of organic carbon. It mainly targets particulate organic carbon (POC). This is because POC, generated by primary production (Phytoplankton), is heavier than sea water and thus sinks (Mahadevan 2014). Additionally, POC generated at the surface ocean can also be transported through the horizontal and vertical advection of surrounding seawater, known as subduction (Stukel et al. 2018).This is the process of fluid transfer from the upper ocean into its deeper interior (Hazeleger & Drijfhout 2000).

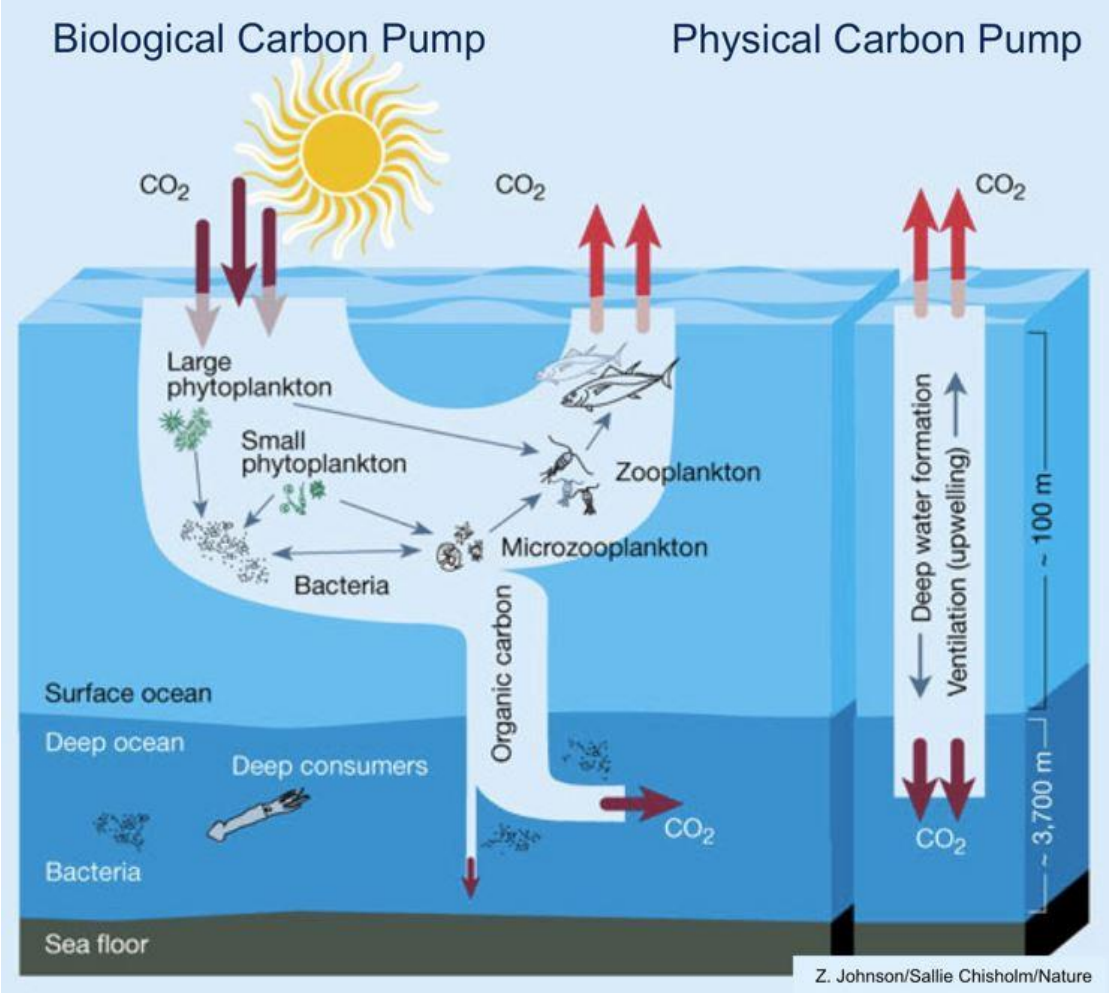

Figure 3. Schematic of the composition of biological oceanic carbon pumps, indicating the sea-air exchange of carbon (Chisholm 2000).

1.4 The impact on carbon export to the deep sea associated with eddies and fronts

It has been argued that subduction is intimately bound up with eddies and fronts. Mahadevan (2014) explored the biogeochemical variation involving the subduction event associated with eddies and fronts on the coast of Peru (Fig 4). Winds blowing along the coast toward the equator drive a flow of surface water that generates upwelling at the coast (Fig 4). The contrast in density between cold upwelling water and warm offshore surface water forms the coastal current, which also moves toward the equator. Upwelling draws nutrients from the deep layer into sunlit areas, where it triggers a rapid growth of phytoplankton creating a biologically productive surface layer. The coastal current is unstable, leading to the occurrence of eddies. Filaments will be generated across the front, with a different density from the surrounding environment (Mahadevan 2014). The denser water from the shore is drawn offshore in the form of filaments, where it is connected to the subsurface water with similar density. This generates a subduction on the inner flanks of the filament, exporting phytoplankton carbon, nutrients and oxygen to the subsurface layer along the isopycnals. These dynamic features affect the fate of POC produced by photosynthesis and thus local biogeochemical budgets (Mahadevan 2014). In this case, the subduction associated with eddies and fronts contributes to the carbon export to the deep sea.

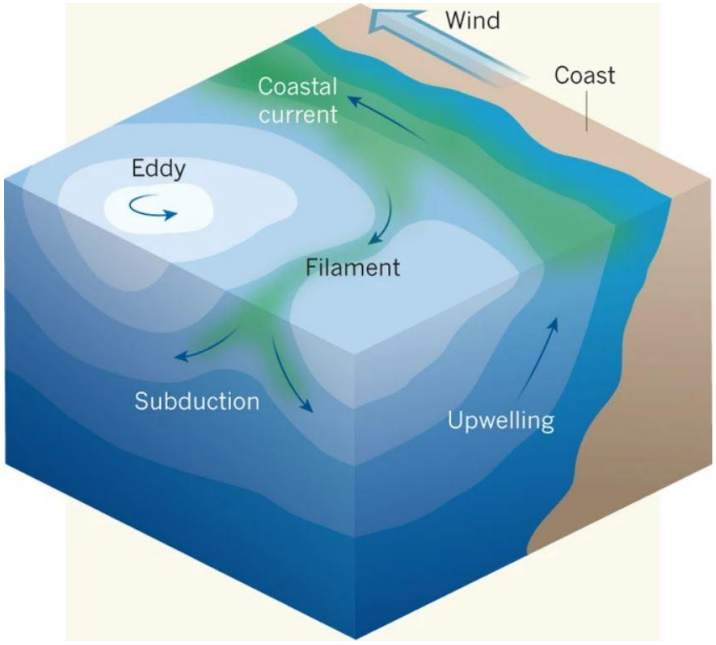

Figure 4. Schematic diagram of the formation of subduction associated with eddies and fronts on the coast (Mahadevan 2014).

Additionally, Xu et al. (2014) explored the effect of mesoscale eddies on the subduction of mode waters in the North Pacific by comparing relevant observations and results of a general ocean circulation model simulation. Their results suggested that mesoscale eddies dramatically increased subduction, contributing up to 50% of the total (subduction) rate. Similarly, Spall (1995) demonstrated that subduction was also accomplished by deep geostrophic circulations which carry the water parcels below and across the front due to baroclinic instability and the resulting frontogenesis. In general, it is evident that subduction is closely associated with eddies and fronts. However, particle export driven by physical subduction acted on diverse spatial and temporal scales, especially small-scale subduction derived by intense vertical circulations involving mesoscale to sub-mesoscale (1-10 km) eddies and frontal circulations (Boyd et al. 2019).

To explore this small-scale spatial effect, it is advantageous to combine the use of towed and autonomous platforms (e.g. gliders, floats, AUVs) with high-resolution models and remote sensing (Guidi et al. 2012). There are already some fine-scale measurements showing that the carbon export can be enhanced at the centre of mesoscale eddies or in their peripheral frontal structure (Resplandy, Lévy & McGillicuddy Jr 2018). The measurements can be traced back to the early 1990s, when Newton et al. (1994) conducted a 17-months study of the spring bloom occurring in the northeast Atlantic, measuring the particulate carbon fluxes to a depth of 3100 m at 45°50′N, 19°30′W, by using time-series sediment traps. They found that the variability in the sediment traps contributes significantly to POC flux. Twenty years later, Stukel et al. (2017) collected numerous samples from mesoscale fronts and used vertical velocities deduced from an ocean circulation model to demonstrate that the subduction contributed to nearly half

of the POC export from the frontal zone. Omand et al. (2015) illustrated that subduction driven by eddies intensifies the export of small and non-sinking POC. They showed subduction driven by eddies to be due to subsurface intrusions of water from the upper mixed layer depth, generated by the enhancement of fronts in the eddy current field. This work was based on autonomous observations from a Seaglider coupled with a high-resolution ocean model. However, there are only a few works that use Triaxus data to investigate the relationship between subduction and particle carbon export. This study will use Triaxus data to explore this relationship.

1.5 Aims

1) Evaluate the quantity of Triaxus data collected by R/V Investigator

2) Evaluate the quality of Triaxus data collected by R/V Investigator

3) Explore Triaxus data to identify fine-scale features, such as subduction events and their relationship with physical oceanographic context.

2. Data and Methods

2.1 Triaxus data acquisition and statistics

This study investigated available Triaxus biogeochemical datasets collected on 15 voyages of the research vessel *RV Investigator* around Australia between early 2015 and late 2019. All datasets were downloaded in netcdf format from the Integrated Marine Observing System (IMOS) website (https://www.marlin.csiro.au). These datasets were identified in the Marlin metadata system by searching for the keyword Triaxus. The data was collected by a range of oceanographic sensors attached to the Triaxus platform which was deployed between the surface and ~ 200-350 metres depth. Sensors included CTD, Dissolved oxygen, Transmissometer, Cosine Photosynthetically Active Radiation (PAR) and ECO Triplet.

In this study, parameters to be used include temperature, salinity, oxygen, chlorophyll,

optical backscatter (OBS), transmissivity and coloured dissolved organic matter (CDOM). The above parameter data was calculated using the Seabird SBE911 CTD 23 in CAP CTD acquisition software, which generated standard data products using data from the primary sensors to produce an along-track time-series dataset for each CAP scan file. These scan files were grouped into sections containing each Triaxus tow. The above process generated the along track data recorded as a function of time. The vertical cast was created by interpolating values from the along track data into consecutive profiles from the sea surface to the maximum dive depth. These two data products were produced by the Marine National Facility (MNF) and made available to download. In this study, we adopted the vertical cast type of Triaxus data, which was easier to process due to its smaller data volume. The collection area of the above datasets was widely distributed in the East Australian Current, the Antarctic Circumpolar Current and Subantarctic Zone near the southeast and south of Tasmania, downstream of the Kerguelen Plateau Islands, the Great Barrier Reef, and the East Indian Ocean around western Australia (Fig 5).

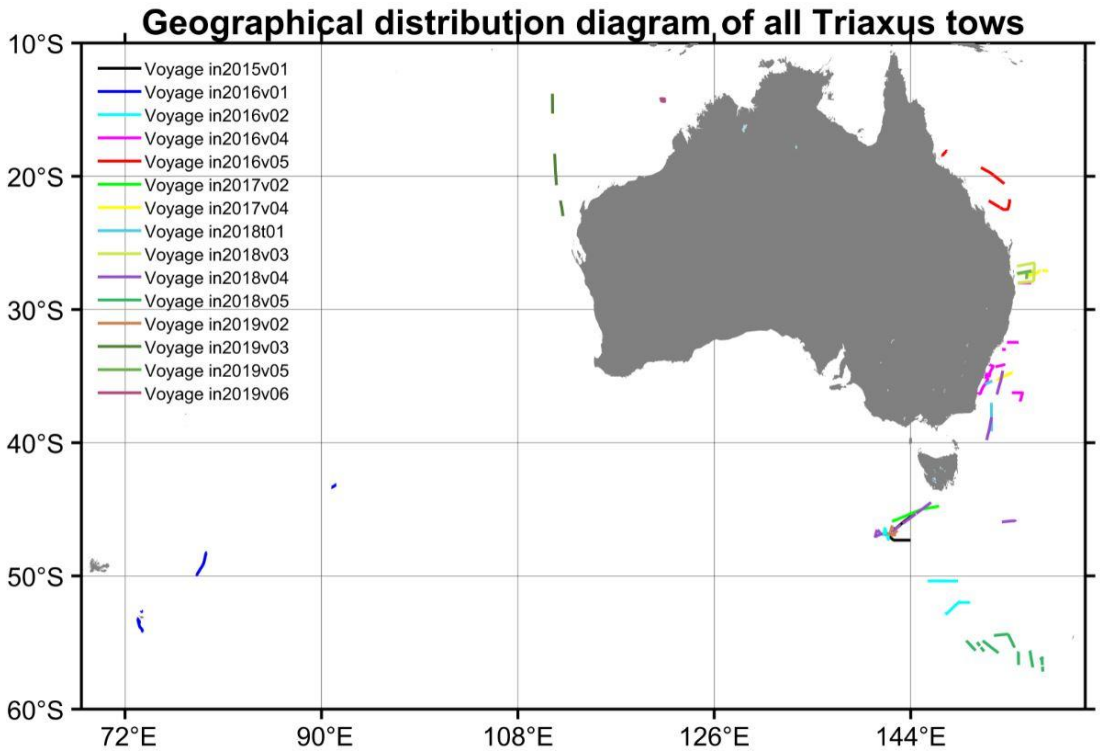

Figure 5. Geographical distribution of the track of all Triaxus tows from 15 voyages

around Australia. Each colour represents a voyage.

Triaxus data including exact time, geographic coordinates, measured biogeochemical parameters data and Quality Control (QC) flags for each tow from each voyage were read in MATLAB. The QC flags for each biogeochemical parameter were visualized to check the corresponding data quality. We also calculated the ratio of QC flags labelled good to the total amount of QC flags collected for each parameter to assess the overall quality of the Triaxus data collected. Data issues revealed through visualization and problems encountered in the working process of sensors for each parameter from the relevant Triaxus data processing report acquired from the Marlin metadata system, were recorded. All the above information was aggregated into a table and displayed in the results section (see Table 1).

We generated basic transect plots of primary parameters for each Triaxus tow including temperature, salinity, dissolved oxygen, chlorophyll, backscatter and transmissivity (Electronic Appendix II), as a visualization for all of Triaxus tows. The above visualization process was accomplished in MATLAB, where the corresponding parameters would not be shown in transect plots if sensors malfunctioned. We characterised each transect plot and identified interesting features associated with the behaviour of chlorophyll and BACKSCATTER occurring underwater, as summarised in the Table 1. In this study, we selected some transects from which interesting features arose, to further explore. For these selected transects, we applied extra scrutiny to the QC flags to highlight low quality data in order to better distinguish them in the transect plot. For example, we excluded data with a QC flag of ‘bad’ or ‘suspect’ when generating a transect plot explored further. Additionally, for the selected transects, we applied additional data products (satellite and Acoustic Doppler Current Profiler (ADCP)) and derived parameters to provide oceanographic context.

2.1.1 CTD measurements (including temperature, salinity and pressure)

Physical parameters including temperature, conductivity and pressure from the selected transects were recorded at a fine-scale vertical resolution and averaged into 1 decibar/10 second bins. This data was collected with the CSIRO CTD unit 23, a Sea-Bird SBE911 with dual conductivity and temperature sensors divided into the primary and secondary sensor. The CSIRO and Sea-Bird-supplied calibration factors were used to compute the pressure, conductivity and temperature data. The data was processed by using quality control to remove spikes and out-of-range values. In this study, temperature and salinity data for each tow was taken from the primary sensor if it was operating properly, otherwise temperature and salinity data from the secondary sensor was used. The data processing report for all of the voyages is available from the CSIRO Marlin metadata system.

Practical salinity and in-situ temperature from Triaxus datasets were converted to absolute salinity (g kg^{-1}) and conservative temperature (°C) respectively. This was done primarily to eliminate the effects of spatial variations in the composition of seawater on seawater properties (such as density and specific volume) which is essential for accurate calculation of salt and heat content (of seawater) (McDougall et al. 2012). It is also important because thermodynamic properties are functions of absolute salinity (rather than of practical salinity) and conservative temperature (rather than of in-situ temperature) according to the Thermodynamic Equation Of Seawater – 2010 (TEOS-10) (Commission 2015). Furthermore, we can study other thermodynamic properties based on these values, including potential density (kg m^{-3}) which was calculated from absolute salinity and conservative temperature. In addition, the latitude and longitude of each tow was converted to a distance in unit of km relative to the initial point of each tow. All the above algorithms were processed in MATLAB using the GSW toolbox acquired from the website (http://www.teos-10.org/software.htm#1).

2.1.2 The Mixed Layer Depth, N^2 and Spiciness

For the determination of the mixed layer depth (MLD), we adopted a judgement standard proposed by de Boyer Montégut et al. (2004) as the depth at which the change of density from a near-surface value at the 10 m depth was 0.03 $kg \cdot m^{-3}$.

The buoyancy (Brunt-Vaisala) frequency squared (N^2) was defined as the follow equation:

$$N^2 = -\frac{g}{\rho_0}\frac{\partial \rho}{\partial z} \quad (1)$$

where g is the gravitational acceleration, ρ_0 is the average density of seawater and $\frac{\partial \rho}{\partial z}$ is the density gradient in the vertical direction, as an indicator reflecting changes of the vertical density gradient in seawater, whose magnitude represented the intensity of fluid stratification (Dohan & Sutherland 2003; Turner 1981). N^2 was calculated by using absolute salinity, conservative temperature, pressure and latitude (used in the determination of gravitational acceleration).

The spiciness was used to distinguish water masses with different temperature and salt properties but similar density (Flament 2002). It was calculated from absolute salinity and conservative temperature at a pressure of 0 dbar (McDougall & Krzysik 2015). All the above algorithms were processed in MATLAB using the GSW toolbox.

2.1.3 Dissolved Oxygen, Chlorophyll, OBS, CDOM, OBS-CHL, attenuation and Apparent Oxygen Utilization

Biological parameters including dissolved oxygen, chlorophyll, backscatter (OBS), CDOM and transmissivity from the selected transects were recorded at a fine-scale vertical resolution and averaged into 1 decibar/10 second bins. The dissolved oxygen data was taken from the primary sensor if it was operating properly, otherwise oxygen data from the secondary sensor was used.

The amount of non-chlorophyll matter was measured using the relative amount of chlorophyll and backscatter. In this case, the in-situ measurement of chlorophyll and backscatter extracted directly from the Triaxus data were normalised with the following formula:

$$x' = \frac{x - \min(x)}{\max(x) - \min(x)} \tag{2}$$

where, x is the magnitude of chlorophyll or backscatter and x' is the magnitude of normalised x.

By taking the difference between them (OBS-CHL), we can find how much particulate matter does not contain chlorophyll, which means it is either dead or processed phytoplankton (i.e. still POC), or other particulate matter such as sediments. The Wetlabs C-Star transmissometer was used for all Triaxus tows to measure transmissivity, where the transmissivity was negatively correlated with chlorophyll and backscatter, indicating that the transmissivity would decrease when chlorophyll and backscatter increased. The attenuation, the sum of absorption and scattering, which directly reflected the amount of particulate matter in seawater, was obtained by the following formula:

$$\text{attenuation} = 100\% - \text{transmissivity} \tag{3}$$

Apparent oxygen utilization (AOU), an important basis for determining the microbial activity in seawater, was calculated as the dissolved oxygen concentration at saturation, given in-situ temperature, salinity and pressure, minus the actual concentration of dissolved oxygen. The dissolved oxygen saturation, was calculated using absolute salinity and conservative temperature coupled with the pressure, longitude and latitude. Calculation was done in MATLAB using gsw_O2sol function from the GSW toolbox. All the above algorithms were processed in MATLAB.

2.2 Acoustic Doppler Current Profiler velocity

Data not from Triaxus were also used, such as the shipboard Acoustic Doppler Current Profiler (ADCP) data and satellite data. The subsurface horizontal ocean velocity data

is given as two components: zonal velocity component u (m s^{-1}) and meridional velocity component v (m s^{-1}). These were collected by the onboard ADCP during the cruise. The ADCP is a sonar-like hydroacoustic current meter that uses the doppler effect of sound waves scattered back from particles in a water column to measure the water velocity within a certain depth range.

The ADCP data for all of the voyages (identified by searching for the keyword ADCP) was downloaded in netcdf format from the CSIRO Marlin metadata system. For data processing, ADCP data was extracted using MATLAB. Real-time information including latitude, longitude, water depth, exact time, u and v were exported. Then ADCP data corresponding to same times the Triaxus was deployed was used. This included a 5-minute bin offset to account for the distance between ship and Triaxus. Additionally, the latitude and longitude from the ADCP data was also converted to km relative to the first full profile in the Triaxus plot.

There were two ADCPs used for nearly all of the voyages, namely the 150kHz and 75kHz ADCP. The 75kHz ADCP provided data from 30 - ~800 m depth at 16 m recording intervals. The 150kHz ADCP provided data from 30 - ~300-400 m depth at 4 m recording intervals. In order to sample the depth interval equivalent to Triaxus and obtain higher resolution, we use the data from the 150 kHz ADCP. For voyage IN2018T01, because the RDI Ocean Surveyor was out of service, a WorkHorse Quartermaster 150kHz ADCP was used for the duration of the voyage, with both it and the RDI Ocean Surveyor 75kHz ADCP running in narrowband mode during the Triaxus deployment. For voyage IN2016V04, only 150 kHz ADCP data was available for the duration of the voyage, because the 75 kHz ADCP unit was silenced to prevent interference with the 70 kHz single beam instrument (another onboard instrument used on the voyage IN2016V04). The ADCP was operated in narrowband mode for the duration of the voyage. The above information was recorded by the relevant data

processing report from the Marlin metadata system. Here, these two voyages would be further explored in this study. The ADCP data processing report for the voyage IN2018T01 is available at the website: https://www.marlin.csiro.au/geonetwork/srv/eng/search#!f0db179e-6b8b-41ee-ba1e-2316fe0eed82. The ADCP data processing report for the voyage IN2016_V04 is available at the website: https://www.marlin.csiro.au/geonetwork/srv/eng/search#!2f2e73db-b262-4605-8153-6d1ba8f3a319.

2.3 Satellite Data

This study used satellite data from the IMOS website, including sea level anomaly (SLA), sea surface temperature (SST), sea surface chlorophyll-a (Chl-a). All of the above satellite datasets identified by the corresponding keyword were downloaded in netcdf format from the IMOS website (https://portal.aodn.org.au/). The SLA reflected the variation of sea surface height. The SLA data was derived using interpolation of altimeter and tide gauge estimates of sea level. In this study, we use the delayed mode version of SLA data because it the processing includes data collected before and after each map date and so is symmetrical about the map date unlike the near real time SLA data. The SLA data for the time period of each Triaxus tow were sub-sampled. In addition, the surface horizontal geostrophic velocity data (surface geostrophic eastward seawater velocity U (m s^{-1}) and surface geostrophic northward seawater velocity V (m s^{-1})) were provided with the SLA dataset. The surface horizontal geostrophic velocity components were derived from gridded (adjusted) sea level anomaly (GSLA) added to the mean surface velocity (over 18 years of model time) from Ocean Forecasting Australia Model version 3 (OFAM3). The surface geostrophic velocity (m s^{-1}) was then expressed by the sum of sub-vectors U and V.

The SST represented skin temperature of the water body. In this study, we adopted a

daily SST data product that was smoothed with a 6-day running mean, with day time values and night time values averaged separately. The SST data were derived using observations from AVHRR instruments on all available NOAA polar-orbiting satellites. The SST data for the time period of each Triaxus tow were sub-sampled. The SST data is an estimate of the foundation temperature of the upper few meters of the ocean in the absence of diurnal variation. This was directly applied to visualizing SST maps. The unit of SST metadata was kelvin (K), which was converted into the unit of degrees Celcius (℃) through the following equation:

$$\text{SST}\ (℃) = \ \text{SST}\ (\text{k}) - 273.15\ \text{k} \tag{4}$$

The concentration of Chl-a was regarded as a proxy for phytoplankton biomass in seawater (Lalli & Parsons 1997). The Chl-a data downloaded from the IMOS website represented the concentration of inferred Chl-a from relative fluorescence per unit volume of the water body. In this study, we adopted a Chl-a data product where the concentration of Chl-a was estimated by multi-spectral measurements from a MODIS sensor deployed in the Aqua satellite platform combined with the OC3 algorithm (http://oceancolor.gsfc.nasa.gov/cms/atbd/chlor_a). Where possible, we used satellite Chl-a data corresponding to the same day as the Triaxus tows. Where there was too much missing data, we averaged Chl-a data for up to 1 day before and after the date of the tow.

2.4 Eddies and fronts identification

Eddies were identified by SLA data. The warm-core eddy had closed contours of SLA with SLA greater than zero in the centre and the cold-core eddy had closed contours of SLA with SLA less than zero in the centre. The oceanographic area covered by the maxima and minima of sea surface height in the SLA map were considered, respectively, as the centre of warm-core eddies and cold-core eddies. Fronts were identified by SST data coupled with the ADCP data. A front was a strip along the sea surface where sea

surface temperature changed by more than one degree over a distance of ten miles (the distance in km that is equal to 10 miles) (Cromwell & Reid Jr 1956). There are close isotherms and intensively horizontal and vertical motions in the water column around the ocean front in the frontal layer (Cromwell & Reid Jr 1956). Therefore, we could identify the existence of fronts through the visualization of SST from satellite and subsurface horizontal velocity from ADCP.

3. Results

3.1 The summary of Triaxus datasets

This study incorporated 15 Triaxus datasets of interest, collected by the research vessel *RV Investigator* around Australia between 2015 and 2019. The datasets are summarized in the following table.

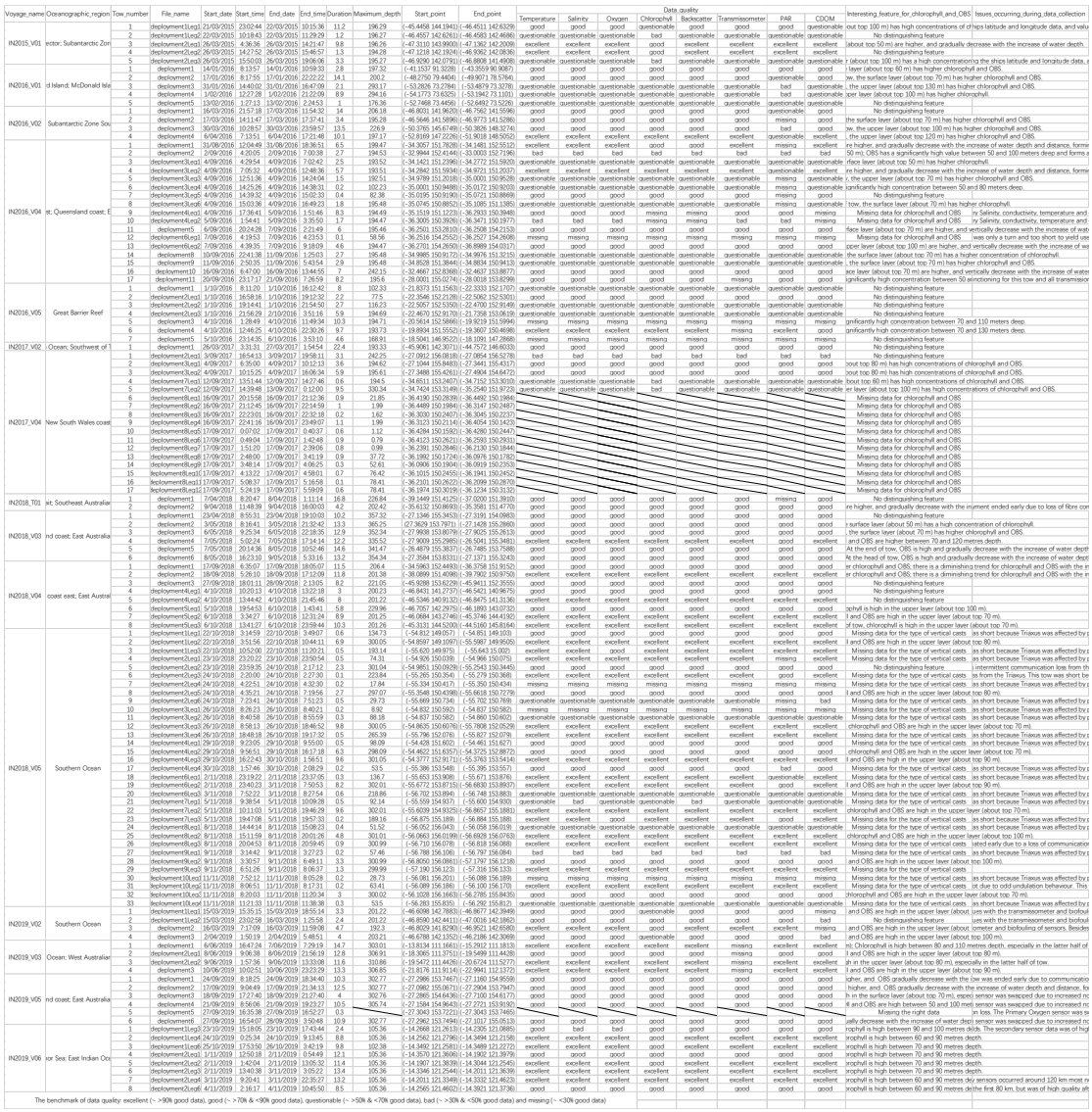

Table 1. A thumbnail of information about each tow from all voyages including voyage name, oceanographic region, tow numbers and their corresponding file names, start date and end date, specific start time and end time, duration, maximum depth, initial and final geographic coordinates, the percentage of data points with the QC flags labelled as good for parameters measured and interesting features about the variation of chlorophyll and backscatter observed from the visualization through Matlab. The slash represents the absence of corresponding data. Based on the calculation of the proportion of data with a QC flag of 'good', the data quality for each sensor is divided into five levels, which respectively are excellent (~ ≥ 90% good data), good (~ ≥ 70% & < 90% good data), questionable (~ ≥ 50% & < 70% good data), bad (~ ≥ 30% & < 50% good data) and missing (~ < 30% good data). The flag "good data" indicates

that there is no error in the measurement (Pender 2000). Please see the Electronic Appendix I for the detailed form.

As can be seen from Table 1, data collection was widely distributed around Australia (Fig 5). The duration of tows ranged from less than an hour to more than 20 hours. The maximum depth of tows ranged from 200 to 350 metres with most tows being around 200 m. Some individual tows did not have available or good quality data due to insufficient duration time and/or maximum depth. These included tows 6-17 of voyage IN2017V04 and 1, 3-4, 6-7, 9-11, 13-14, 17-18, 20-21, 23-24, 26-27, 30-31, 33 of voyage IN2018V05. Additionally, the data from tow 5 of voyage IN2019V05 was the same as that of tow 1 due to an error in publishing in the Marlin metadata system (https://www.marlin.csiro.au/geonetwork/srv/eng/search#!0b726b36-c06e-4d16-b9ff-c9963e8ba9b5). For the above special tows, the unavailable information was marked as a slash in Table 1.

Data quality, recorded by QC flags, was generally good for the temperature, salinity, oxygen, chlorophyll, backscatter, transmissometer, PAR and CDOM; however, some individual data was corrupted due to issues such as noise, problems with manual operation, breakdown of sensors, and interference from marine life. For specific reasons, please refer to the Electronic Appendix II for Triaxus processing reports of each voyage.

After creating visualisations of all of the Triaxus tows, we examined the chlorophyll and OBS plots in search of "interesting features" such as the change in values of these variable between the surface and the deeper water. An example of this was seen in the transect of the 2nd tow from voyage IN2018_T01. Here there is an obvious gradual decrease in the concentration of chlorophyll and OBS toward the deeper ocean (see Fig 9), which has the appearance of suspected subduction events reported in the literature (Mahadevan 2014). Similar phenomena, where chlorophyll and OBS can be seen

penetrating into deeper water with a trend of gradual decrease were observed in the profiles of the 1st , 2nd and 3rd tows from voyage IN2016V04 (see Figs 15, 21 & 27). It is worth mentioning that these tows were the most representative examples in the EAC region, namely the most obvious subsurface biomass features identified as "suspected subduction events". Other tows had some similar but less obvious features, which might need exploration in future work.

3.2 Study Region for voyages IN2018T01 and IN2016V04

The 4th aim of this study focused on 4 Triaxus tows located in the EAC region (Figs 6 & 7). For voyage IN2018T01, we focused on the 2nd tow which passed through the edge of a small cold-core eddy (Fig 6), called ‘eddy 1’, where the direction of geostrophic velocity around eddy 1 was clockwise.

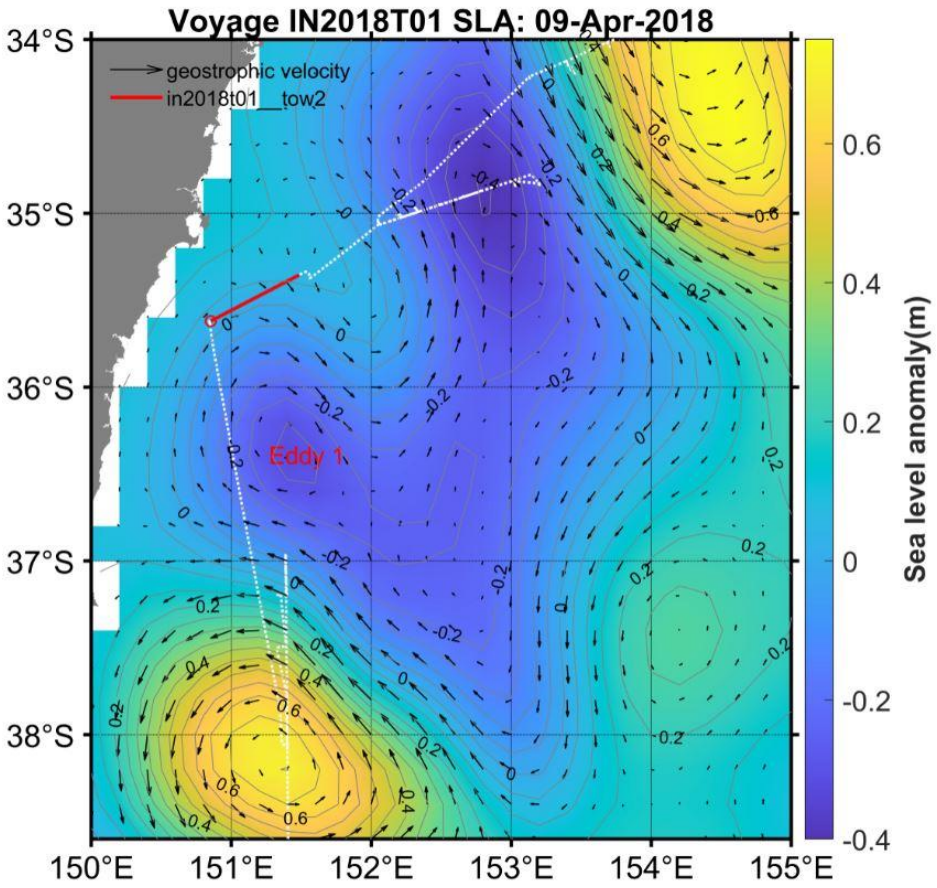

Figure 6. Map of the study region for voyage IN2018T01 along the East Australian Current (EAC), where background colours represent the Sea Level Anomaly (SLA) and

background contour lines represent the sea surface height. White dotted line represents the track of the voyage IN2018T01. The direction and size of black arrows respectively represent the direction and magnitude of surface geostrophic velocity. The red solid lines represent the track of the 2nd tow during the voyage, which passes through the edge of an eddy whose centre is marked as Eddy 1 in red. Yellow circular regions of positive SLA indicate warm-core eddies while blue circular regions of negative SLA indicate cold-core eddies. Sea level anomaly and sea level height in this map are averaged between the 30th of August and the 4th of September 2016. Data are downloaded from the Integrated Marine Observing System (IMOS).

For voyage IN2016V04, we focused on the 1st, 2nd and 4th tows. There were two eddies including a warm-core eddy (called 'eddy 2') and a cold-core eddy (called 'eddy 3') near these tows (Fig 7). The 1st tow of this voyage passed through the edges of eddies 2 and 3. The 2nd tow of this voyage passed through the edge of eddy 2. The 4th tow of this voyage passed through the edge of eddy 3.

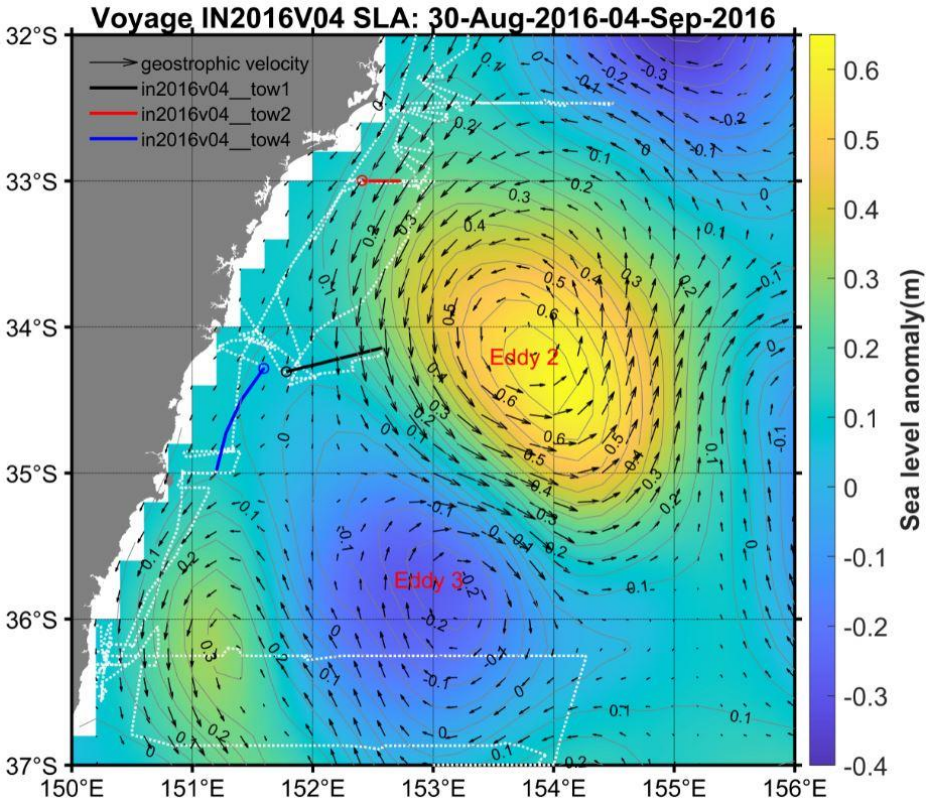

Figure 7. Map of the study region for voyage IN2016V04 along the East Australian

Current (EAC), where background colours represent the Sea Level Anomaly (SLA) and background contour lines represent the sea surface height. White dotted line represents the track of the voyage IN2016V04. The direction and size of black arrows respectively represent the direction and magnitude of surface geostrophic velocity. The black solid line represents the track of the tow 1 during the voyage which passing through the edges of an eddy whose centre is marked as Eddy 2 in red and an eddy whose centre is marked as Eddy 3. The red solid line represents the track of the tow 2 passing through the edge of eddy 2. The blue solid line represents the track of the tow 4 passing through the edge of eddy 3. Yellow circular regions of positive SLA indicate warm-core eddies while blue circular regions of negative SLA indicate cold-core eddies. Sea level anomaly and sea level height data between the 30th of August and the 4th of September 2016 are downloaded from the Integrated Marine Observing System (IMOS).

3.3 Transect plots for the 4 tows

3.3.1 Voyage IN2018T01 tow 2

Vertical profiles of physical parameters along the transect of the 2nd tow from the voyage IN2018T01 showed the variations of six physical variables with depth and distance (Fig 8). Below the MLD, density increased rapidly from 24.4 to 26.4 kg/m^3, with the water depth, and isopycnals were very close together in this upper layer (about top 90 m). This was especially true at along-track distances between 10 and 40 km, indicating there was the greater density gradient than elsewhere in this area (Fig 8d). Furthermore, the distribution of isotherms with water depth was very similar to that of the isopycnals (Fig 8a).

The distribution of salinity was similar to that of temperature (Fig 8b). The distribution of spiciness was also very similar to that of density and variations of spiciness were almost coincident with the isopycnals (Fig 8e). The dissolved oxygen decreased rapidly with depth in the upper layer (about top 100 m), especially at the point where the

isopycnals were close together, and then slightly increased with increasing water depth between 5 and 50 km along the track, where the density gradient decreased gradually (Fig 8c). Additionally, we found that there was some abnormally high dissolved oxygen between the isopycnals of 26 and 26.5 kg/m^3. N^2 was elevated near the MLD where the isopycnals were close together in the upper layer (about top 50 m) (Fig 8f).

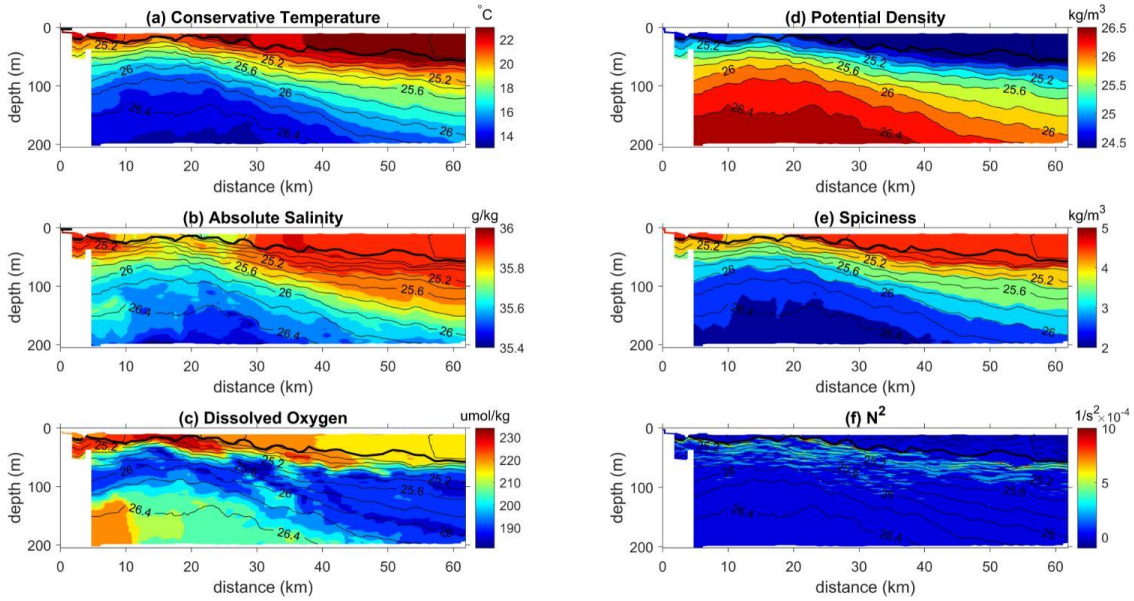

Figure 8. Vertical profiles of physical parameters varying with depth from 0 to 200 m along the transect of the 2nd tow from the voyage IN2018T01 including (a) conservative temperature (℃), (b) absolute salinity (g/kg), (c) dissolved oxygen (μmol/kg), (d) potential density (kg/m^3), (e) spiciness (kg/m^3) and (f) N^2 (1/s^2×10^{-4}). The black contour lines represent the isopycnals and the increment among the isopycnals is 0.2 kg/m^3. The black bold line represents the MLD. The suspect data marked by the black horizontal line near 0 m depth (panels a and b) are only in the first ~ 2km of the transect.

The chlorophyll concentration varied from 0.1 to 0.6 μg/L above the MLD (Fig 9b). The maximum chlorophyll concentration, 0.7-1.3 μg/L, was observed below the MLD (about top 25-50 m) between 9 and 23 km along track, where isopycnals were very close together (Fig 9b). Moreover, the concentration of chlorophyll gradually decreased with depth along the isopycnals, varying rapidly when the isopycnals became denser. Below the MLD, the OBS had a maximum in the upper layer (about top 60 m) between

8 and 25 km, and gradually decreased with depth along the isopycnals (Fig 9a). Here, the black line indicates where data were suspect and were not considered (Figs 9a & 9c). Significantly, the OBS was abnormally high between 20 and 40 km along track in the deeper layer (about 110-190 m), seen as a 'triangular' area. There was a red strip zone in the OBS-CHL between the isopycnals of 26 and 26.4 kg/m^3 at distances between 20 and 40 km, which indicated that the relative amount of OBS was greater than that of chlorophyll (Fig 9c). This was especially the case in the area with abnormally high value of OBS, where the chlorophyll dominated at distances between 20 and 30 km, and at the upper layer of the isopycnal with the density of 26.2 kg/m^3 between 30 and 40 km, while the non-chlorophyll matter dominated at the lower layer of the isopycnal (Fig 9c).

The underwater distribution of attenuation was similar to that of OBS and chlorophyll in the upper layer (about top 50 m) between 10 and 30 km with the attenuation gradually decreasing with depth along the isopycnals between 20 and 30 km (Fig 9d). However, the attenuation was high between 30 and 50 km (Fig 9d) even though both the OBS and chlorophyll were low in this area. It seemed likely there was something wrong with the transmissometer data, as the OBS data at least looked like the chlorophyll data (Figs 9a & 9b).

The AOU was almost constant above the MLD. However, below the MLD, AOU increased rapidly in the upper layer (about top 90 m) where isopycnals were very close together (Fig 9e). Additionally, there was the high AOU in the 'triangular' area where OBS was obviously high (Fig 9e). The subsurface distribution of AOU and CDOM had similar patterns, and high CDOM was found where the AOU was high (Figs 9e & 9f).

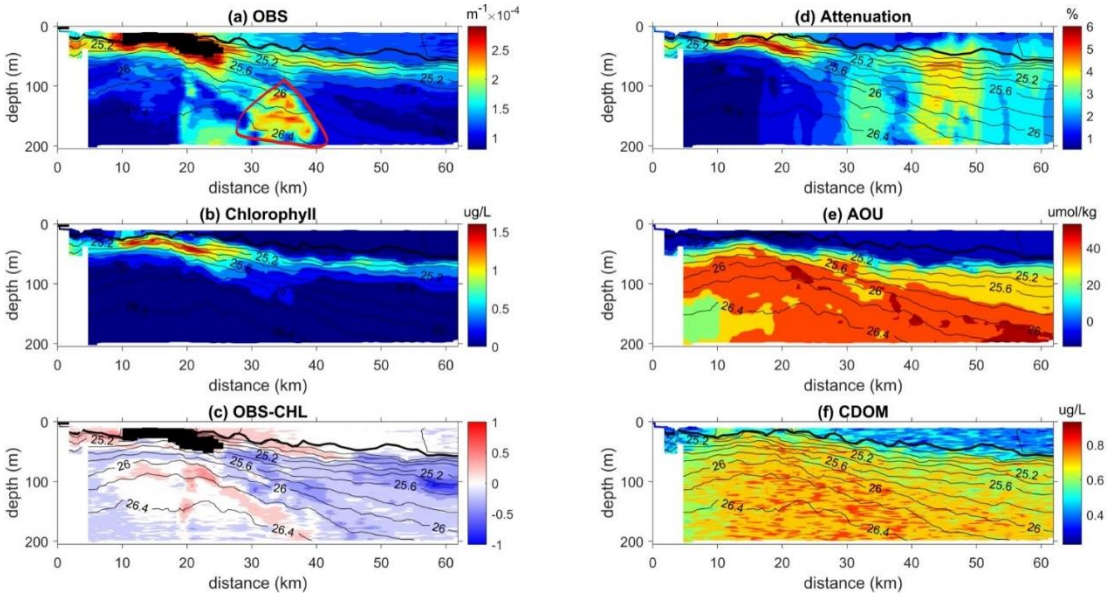

Figure 9. Vertical profiles of biological parameters varying with depth from 0 to 200 m along the transect of the 2nd tow from voyage IN2018T01 including (a) OBS ($m^{-1}\times10^{-4}$), (b) chlorophyll (μg/L), (c) OBS-CHL, (d) attenuation (%), (e) AOU (μmol/kg) and (f) CDOM (μg/L). The black contour lines represent the isopycnals and the increment among the isopycnals is 0.2 kg/m^3. The black bold line represents the MLD. The red line indicates a 'triangular' area where high OBS are observed. The QC flags of data points, covered by the black areas, showed these to be suspect data.

The following vertical profile along the transect of tow 2 shows the subsurface variation of horizontal ocean velocity with depth and distance measured with the shipboard ADCP (Fig 10). Both velocity u-component and v-component were the highest in the upper layer (about top 50 m) between 10 and 30 km and gradually decreased with depth along the isopycnals, varying rapidly at the areas where the isopycnals were close together (Figs 10a & 10b). The velocity u-component and v-component were respectively positive and negative along most of the transect, which indicated that the horizontal velocity zonal component and meridional component were respectively eastward and southward. Note that the triangular region identified from OBS sits below the region where the horizontal gradient of velocity is strongest.

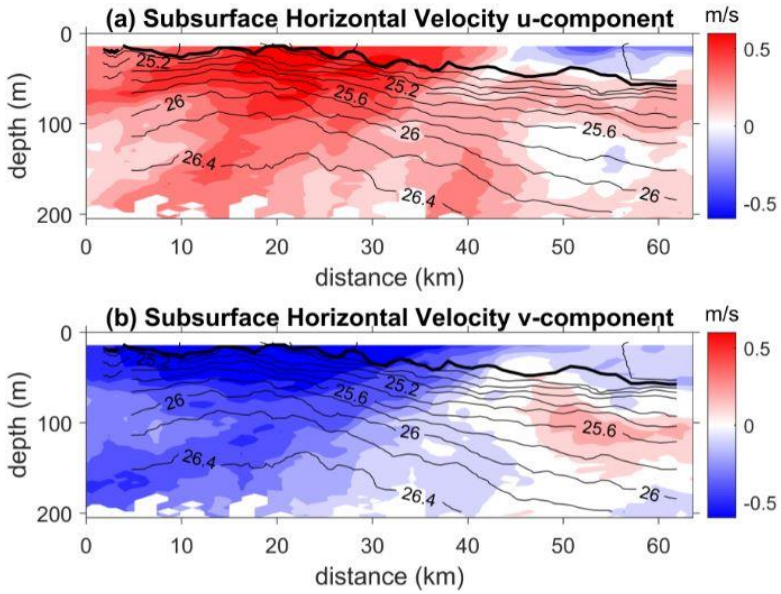

Figure 10. Vertical profiles of subsurface horizontal velocity varying with depth from 0 to 200 m along the transect of the 2nd tow from the voyage IN2018T01 including (a) subsurface horizontal velocity u-component (geographic E component) (m/s) and (b) subsurface horizontal velocity v-component (geographic N component) (m/s). The black contour lines represent the isopycnals and the increment among the isopycnals is 0.2 kg/m^3. The black bold line represents the MLD.

3.3.2 Voyage IN2016V04 tow 1

Vertical profiles of physical parameters along the transect of the 1st tow from the voyage IN2016V04 shows the variations of six physical variables with depth and distance along the transect (Fig 11). The density gradient was small and isopycnals were generally far apart. The density increased from 25.2 to 26.4 kg/m^3 with the water depth below the MLD (Fig 11d). Meanwhile, the subsurface distribution of isotherms with the water depth was very similar to that of the isopycnals (Fig 11a). The temperature decreased gradually with increasing density below the MLD.

The subsurface distribution of salinity was similar to that of temperature (Fig 11b). The variation trend of spiciness was also very similar to that of density and the variation gradient line of spiciness was most close to isopycnals (Fig 11e). In comparison to the

distribution pattern of salinity, spiciness was more similar to temperature and density. Dissolved oxygen decreased gradually along the isopycnals and there was a filamentary pattern downward at the point of 50 km (Fig 11c). In addition, N^2 was significantly high below the MLD where isopycnals were close together, especially along between the isopycnals of 25.8 and 26 kg/m^3 (Fig 11f).

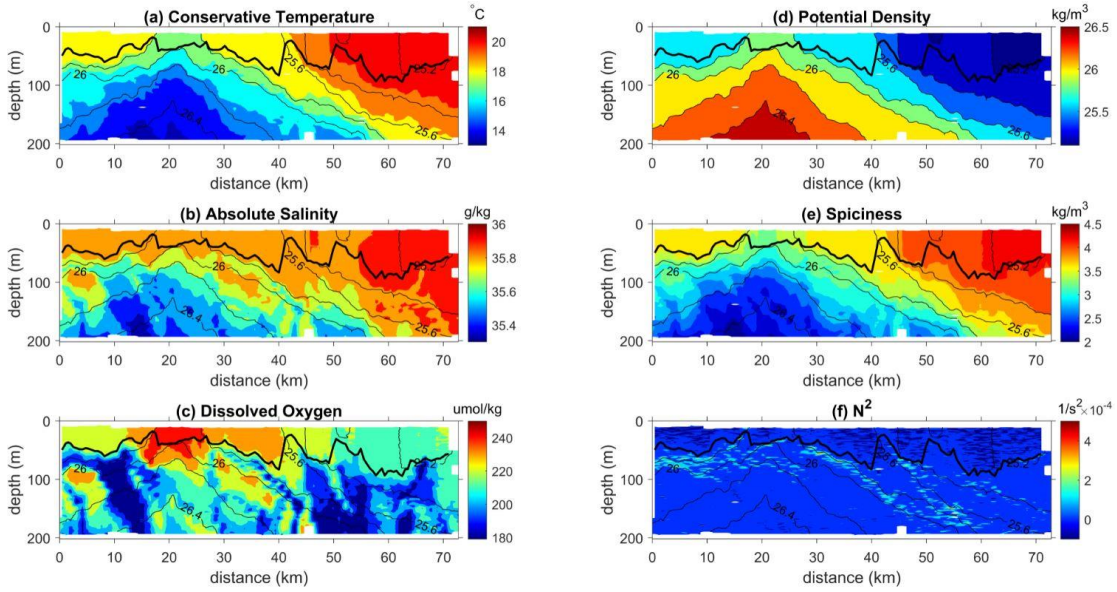

Figure 11. Vertical profiles of physical parameters varying with depth from 0 to 200 m along the tow 1 from voyage IN2016V04 including (a) conservative temperature (°C), (b) absolute salinity (g/kg), (c) dissolved oxygen (μmol/kg), (d) potential density (kg/m^3), (e) spiciness (kg/m^3) and (f) N^2 (1/s^2×10^{-4}). The black contour lines represent the isopycnals and the increment among the isopycnals is 0.2 kg/m^3. The black bold line represents the MLD.

Chlorophyll showed high concentrations, ranging between 0.6 to 0.9 ug/L above the MLD between 30 and 50 km (Fig 12b). Here, the black part represented the suspect data that was not used (Figs 12a, 12b & 12c). The concentration of chlorophyll decreased gradually with depth along the isopycnals (Fig 12b). OBS showed a similar trend. This variable had the highest value above the MLD between 30 and 50 km, and gradually decreased with depth along the isopycnals (Fig 12a). Significantly, the OBS was abnormally high between 50 and 55 km in the deeper layer (about bottom 90-190

m), in the ‘cone’ area (Fig 12b). The OBS-CHL was almost negative in the area of highest concentration of chlorophyll and OBS between 30 and 45 km (Fig 12c), which indicated that the relative amount of chlorophyll was greater than that of OBS. However, in the ‘cone’ area, the amount of OBS dominated (Fig 12c). Whereas, the chlorophyll was dominant in the small part of ‘cone’ area where a filamentary pattern of dissolved oxygen occurred. The underwater distribution of attenuation was similar to that of OBS in the upper layer (about top 50 m) between 15 and 50 km, with the attenuation gradually decreasing with depth along the isopycnals (below the MLD) (Fig 12d). Significantly, the attenuation was abnormally high in the vertical band between 4 and 10 km (Fig 12d). Although this data appeared anomalous the QC flags did not pick this up.

The AOU was almost constant at the upper layer of the MLD and increased rapidly below the MLD (Fig 12e). High AOU corresponded to low dissolved oxygen. Significantly, the subsurface distributions of AOU and CDOM were quite similar (Figs 12e & 12f). Also high CDOM was found where the AOU was high.

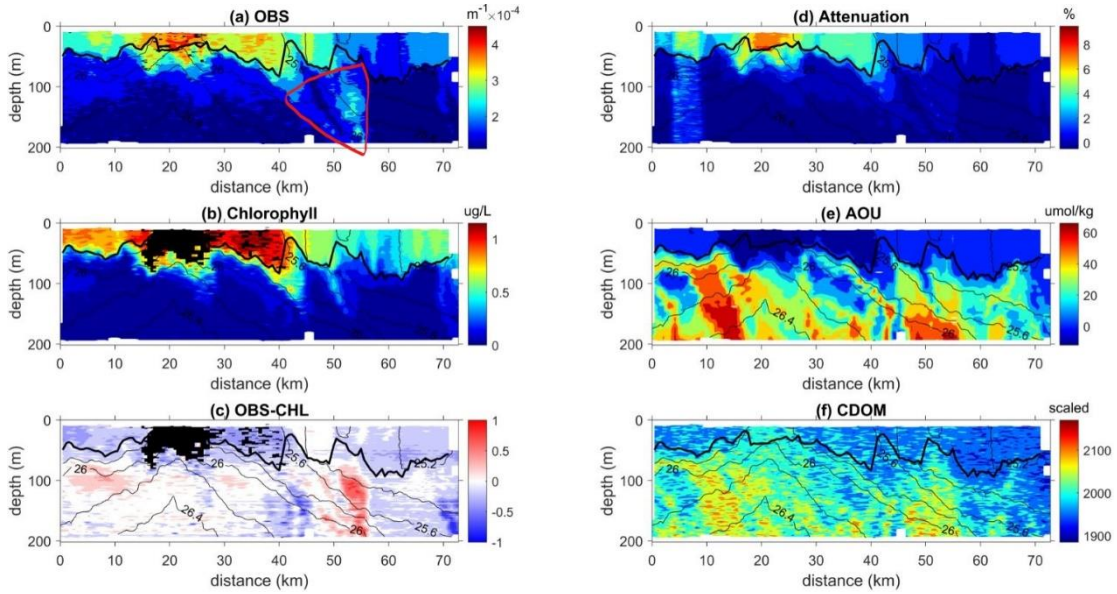

Figure 12. Vertical profiles of biological parameters varying with depth from 0 to 200 m along the transect of the 1st tow from the voyage IN2016V04 including (a) OBS ($m^{-1}\times10^{-4}$), (b) chlorophyll (µg/L), (c) OBS-CHL, (d) attenuation (%), (e) AOU (µmol/kg)

and (f) CDOM (scaled). The black contour lines represent isopycnals and the increment among the isopycnals is 0.2 kg/m^3. The black bold line represents the MLD. The red line indicates a 'cone' area where high OBS are observed. The QC flags of data points covered by the pink areas were suspect.

Both velocity u-component and v-component were highest in the upper layer (about top 50 m) between 10 and 40 km and gradually decreased to zero (with depth) along the isopycnals between 40 and 60 km, varying rapidly in the areas where the isopycnals were close together (Figs 13a & 13b). We also found that u-component and v-component were respectively positive and negative along most of the transect, which indicated that the horizontal velocity zonal component and meridional component were respectively eastward and southward.

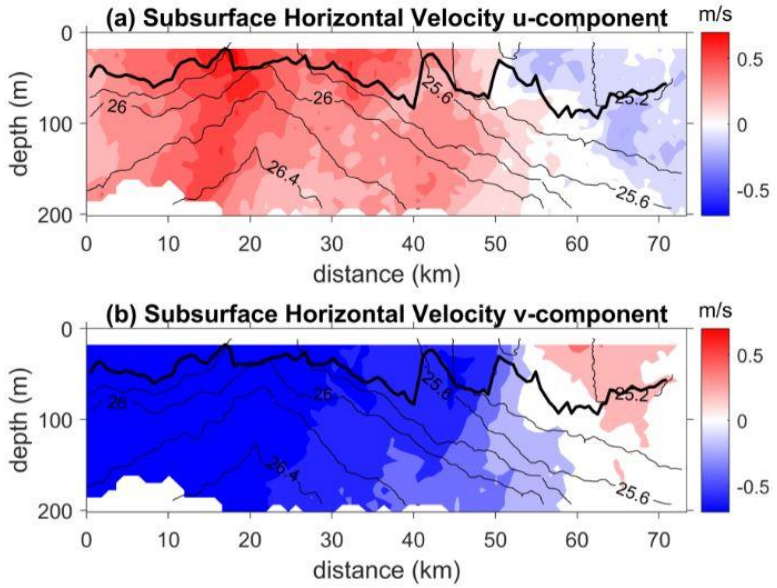

Figure 13. Vertical profiles of subsurface horizontal velocity varying with depth from 0 to 200 m along the transect of the 1st tow from the voyage IN2016V04 including (a) subsurface horizontal velocity u-component (m/s) and (b) subsurface horizontal velocity v-component (m/s). The black contour lines represents the isopycnals and the increment among the isopycnals is 0.2 kg/m^3. The black bold line represents the MLD.

3.3.3 Voyage IN2016V04 tow 2

Vertical profiles the 2nd tow from the voyage IN2016V04 show the variations of six physical variables with depth and distance along the transect (Fig 14). Density was almost constant at the upper layer of the MLD. Below the MLD, density increased slowly from 25.2 to 26.2 kg/m^3 with the water depth (Fig 14d). The subsurface distribution of isotherms with the water depth was very similar to that of the isopycnals (Fig 14a). Similarly, the temperature was almost constant at the upper layer of the MLD decreasing gradually with increasing density below the MLD (Fig 14a). The subsurface distribution of salinity was similar to that of temperature (Fig 14b). The variation tendency of spiciness was also very similar to that of density, temperature and salinity. The variation gradient line of spiciness almost coincided with the isopycnals (Fig 14e). Generally, the subsurface patterns of temperature, salinity, density and spiciness were well-structured.

The dissolved oxygen decreased rapidly as the density gradient became greater, especially at the distances of 6 km and 17 km where the isopycnals were very close together (Fig 14c). An interesting phenomenon showing high dissolved oxygen from the surface layer (about top 40 m) penetrating into the deep sea in a ‘tongue’ shape along the isopycnals, was observed between 8 and 12 km (Fig 14c). Additionally, N^2 was significantly high below the MLD where the isopycnals were close together at a depth of 100 m. N^2 was very small in the same ‘tongue’ area as the dissolved oxygen (Fig 14f).

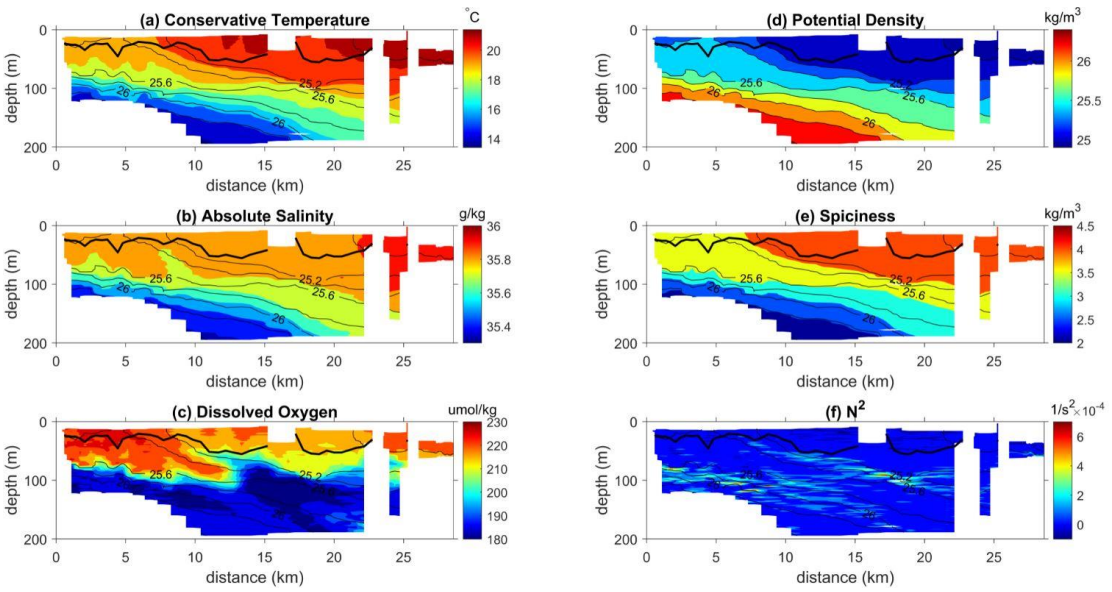

Figure 14. Vertical profiles of physical parameters varying with depth from 0 to 200 m along the transect of the 2nd tow from voyage IN2016V04 including (a) conservative temperature (℃), (b) absolute salinity (g/kg), (c) dissolved oxygen (μmol/kg), (d) potential density (kg/m^3), (e) spiciness (kg/m^3) and (f) N^2 (1/s^2×10^{-4}). The black contour lines represents the isopycnals and the increment among the isopycnals is 0.2 kg/m^3. The black bold line represents the MLD.

There was also a similar 'tongue' area showing high values of OBS, observed between the isopycnals of 25.4 and 25.6 kg/m^3 at distances between 7 and 13 km (Fig 15a). The OBS in this area gradually decreased with depth along the isopycnals (Fig 15a). Chlorophyll also showed a similar 'tongue' area extending deeper along the isopycnals, however it was closer to the surface than that of OBS (Figs 15a & 15b). Furthermore, chlorophyll had high concentrations, with the average value of 0.7 ug/L, above the MLD (about top 25-50 m) between 10 and 25 km. Significantly, the OBS-CHL reflected that the OBS dominated within the 'tongue' area indicating the relative amount of OBS was greater than that of chlorophyll (Fig 15c). The subsurface distribution of attenuation was similar to that of OBS in the upper layer (about top 50 m) between 10 and 30 km gradually decreasing with depth along the isopycnals (Fig 15d). Both attenuation and OBS were highest in the upper layer (about top 40-100 m) between 7

and 13 km.

The AOU was almost constant at the upper layer of the MLD (Fig 15e). Below the MLD, AOU increased rapidly at the depth of 110 m where the isopycnals were very close together. Significantly, the 'tongue' area with high concentrations of dissolved oxygen, was also seen in the AOU (Figs 14c & 15e). As was seen with the previous tows, distributions of AOU and CDOM were very similar (Figs 15e & 15f). Furthermore, as we can see from the figure 21f, high CDOM was found where the AOU was also high.

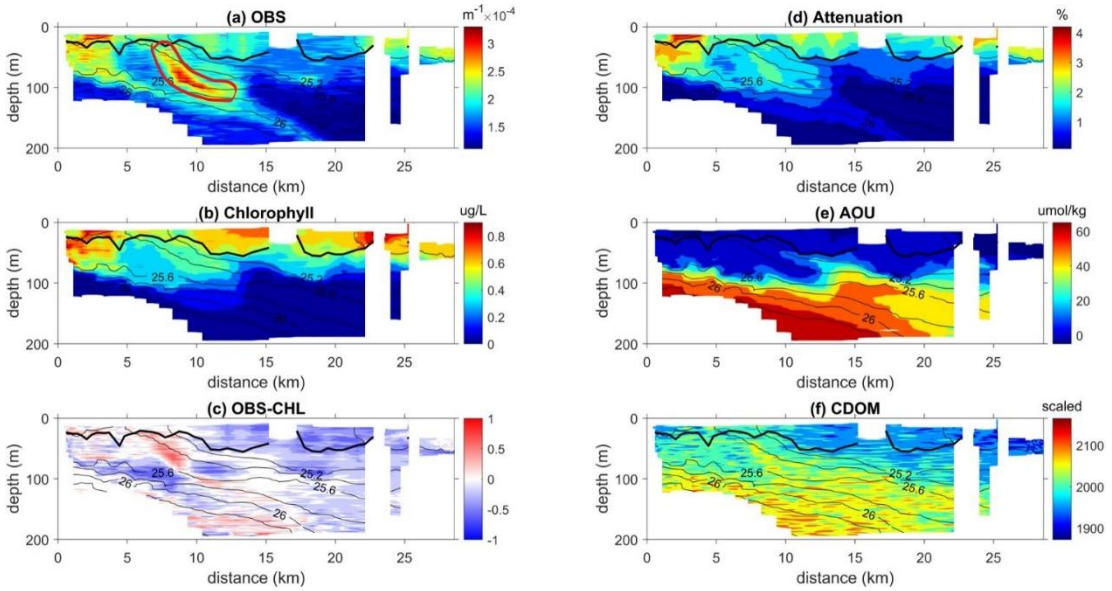

Figure 15. Vertical profiles of biological parameters varying with depth from 0 to 200 m along the transect of the 2nd tow from the voyage IN2016V04 including (a) OBS ($m^{-1}\times10^{-4}$), (b) chlorophyll (µg/L), (c) OBS-CHL, (d) attenuation (%), (e) AOU (µmol/kg) and (f) CDOM (scaled). The black contour lines represent the isopycnals and the increment among the isopycnals is 0.2 kg/m^3. The black bold line represents the MLD. The red line indicates a 'tongue' area where high OBS was observed.

Both subsurface horizontal ocean velocity u-component and v-component were highest in the upper layer (about top 160 m) between 10 and 30 km and gradually decreased with depth along the isopycnals, varying rapidly at the distances between 15 and 20 km

(Figs 16a & 16b). We also found that both the u-component and v-component were negative, indicating the horizontal velocity zonal component and meridional component were respectively westward and southward.

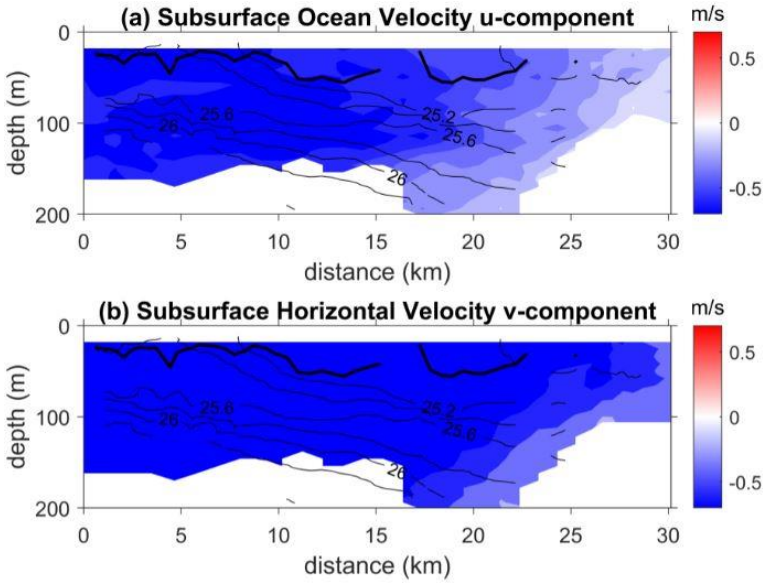

Figure 16. Vertical profiles of subsurface horizontal velocity varying with depth from 0 to 200 m along the transect of the 2nd tow from the voyage IN2016V04 including (a) subsurface horizontal velocity u-component (m/s) and (b) subsurface horizontal velocity v-component (m/s). The black contour lines represent the isopycnals and the increment among the isopycnals is 0.2 kg/m^3. The black bold line represents the MLD.

3.3.4 Voyage IN2016V04 tow 4

Vertical profiles of the 4th tow from the voyage IN2016V04 show the variations of six physical variables with depth and distance along the transect (Fig 17). Density was almost constant at the upper layer of the MLD. Below the MLD, density increased rapidly from 25.6 to 26.2 kg/m^3 with water depth. The isopycnals were very close together, indicating a greater density gradient here than elsewhere in water column (Fig 17d). The distribution of isotherms was very similar to that of the isopycnals (Fig 17a). Temperature was very nearly constant at the upper layer of the MLD and decreased gradually with increasing density below the MLD. Underwater distribution of salinity was similar to that of temperature, but there was still a little difference between the

surface variation in salinity and temperature (Fig 17b). The variation tend of spiciness was also very similar to that of density with the variation gradient line almost coinciding with the isopycnals (Fig 17e). Overall, the subsurface variation of temperature, salinity, density and spiciness were well-structured.

Dissolved oxygen gradually decreased below the MLD, especially where the isopycnals were closer together (Fig 17c). It is worth noting that the dissolved oxygen and salinity seemed to show similar subsurface variability. In addition, N^2 was significantly high below the MLD where the isopycnals were close together in the upper layer (about top 50 m) (Fig 17f).

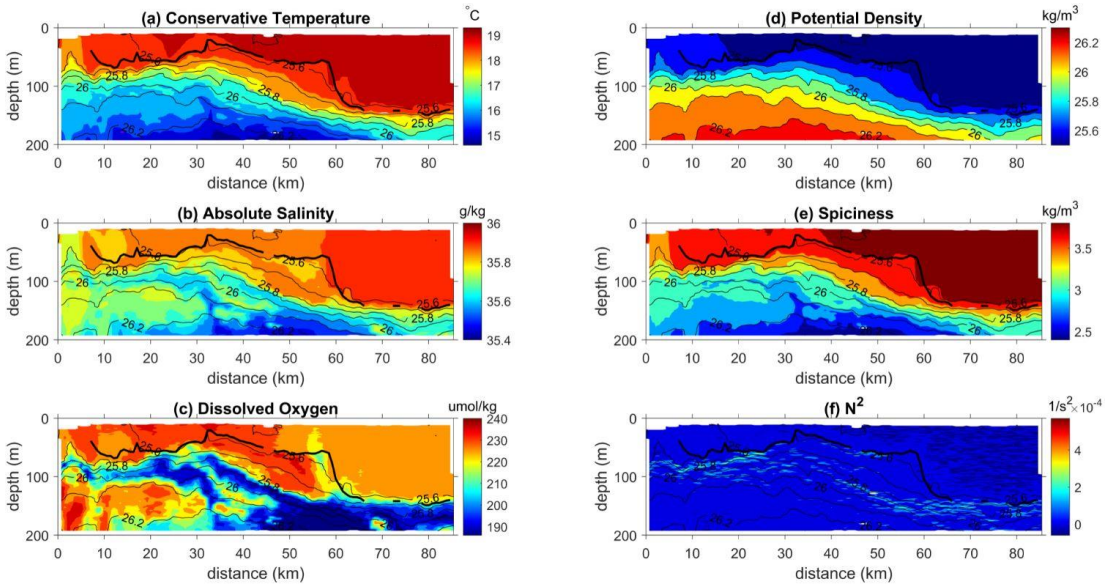

Figure 17. Vertical profiles of physical parameters varying with depth from 0 to 200 m along the transect of the 4th tow from the voyage IN2016V04 including (a) conservative temperature (℃), (b) absolute salinity (g/kg), (c) dissolved oxygen (μmol/kg), (d) potential density (kg/m^3), (e) spiciness (kg/m^3) and (f) N^2 (1/s^2×10^{-4}). The black contour lines represent the isopycnals and the increment among the isopycnals is 0.1 kg/m^3. The black bold line represents the MLD.

Chlorophyll had a high concentration with values ranging from 0.6 to 0.9 ug/L above the MLD (about top 10-50 m) between 5 and 50 km (Fig 18b). Below the MLD, the

concentration of chlorophyll gradually decreased with depth along the isopycnals (Fig 18b). Likewise, the OBS showed a similar trend to chlorophyll. The OBS had a maximum in the upper layer (about top 10-50 m) between 15 and 40 km, and gradually decreased with depth along the isopycnals (Fig 18a). This could be interpreted to mean that the particles observed were transported into the deep sea, as observed by the high value of OBS at the lower layer of the MLD (about bottom 130-190 m) between 31 and 72 km, in a 'strip' like area. A distinguishing feature of this transect, was how chlorophyll, OBS and absorption did not change abruptly at the MLD between 30 and 50 km. Furthermore, in the 'strip' area, the OBS-CHL was positive, which indicated the relative amount of OBS was greater than that of chlorophyll (Fig 18c). Significantly, the region of very low OBS-CHL at the upper layer (about 110-130 m) of the MLD between 60 and 70 m, indicates chlorophyll but little OBS. Additionally, the underwater distribution of attenuation was similar to that of OBS and this attenuation gradually decreased with depth along the isopycnals between 20 and 30 km (Figs 18a & 18d).

The AOU was almost constant at the upper layer of the MLD (Fig 18e). However, AOU increased rapidly below the MLD (about bottom 80-190 m) where the isopycnals were very close together and AOU was high in the corresponding 'strip' area. Significantly, the AOU and CDOM had almost similar patterns which indicates their distribution was very similar (Figs 18e & 18f). In this case, high CDOM was found where the AOU was high.

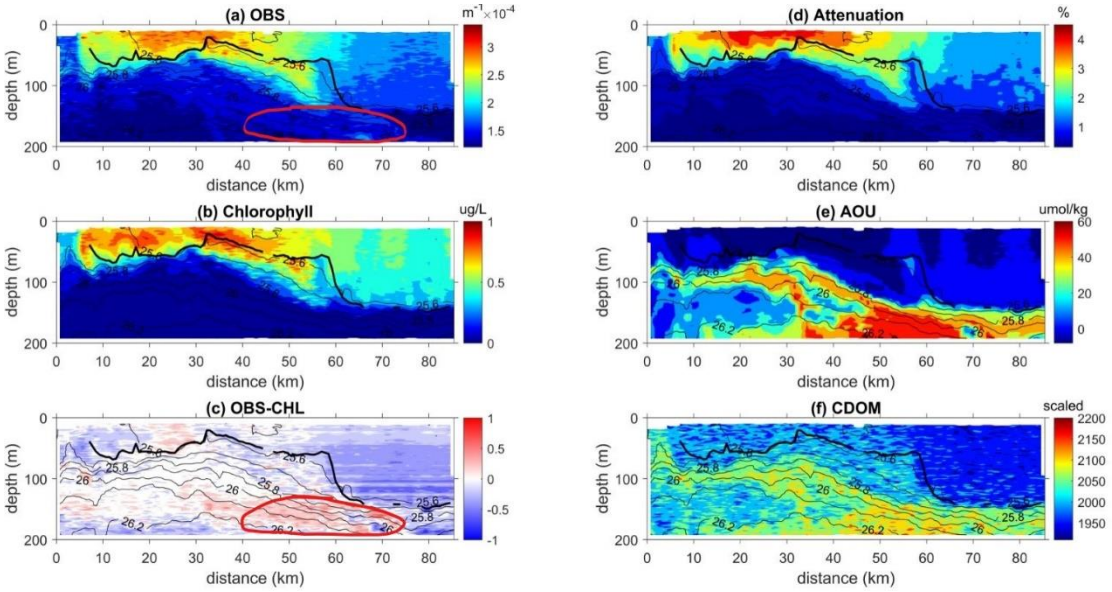

Figure 18. Vertical profiles of biological parameters varying with depth from 0 to 200 m along the transect of the 4th tow from the voyage IN2016V04 including (a) OBS ($m^{-1}\times10^{-4}$), (b) chlorophyll (μg/L), (c) OBS-CHL, (d) attenuation (%), (e) AOU (μmol/kg) and (f) CDOM (scaled). The black contour lines represent the isopycnals and the increment among the isopycnals is 0.1 kg/m^3. The black bold line represents the MLD. The red line indicates a 'strip' area where high OBS are observed.

Both velocity u-component and v-component were highest in the upper layer (about top 150 m) between 10 and 30 km, gradually decreasing to zero and then increasing with depth along the isopycnals. Variation was lowest in the areas where the isopycnals were close together (Figs 19a & 19b).

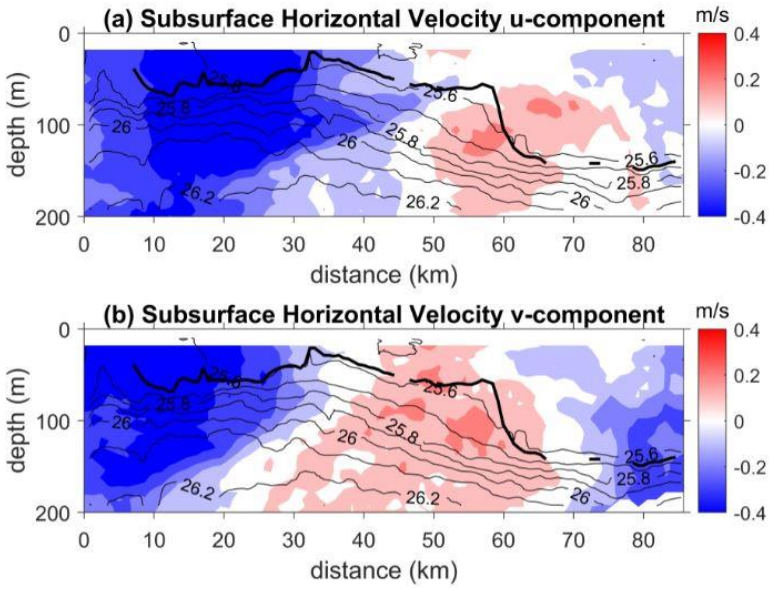

Figure 19. Vertical profiles of subsurface horizontal velocity varying with depth from 0 to 200 m along the transect of the 4th tow from the voyage IN2016V04 including (a) subsurface horizontal velocity u-component (m/s) and (b) subsurface horizontal velocity v-component (m/s). The black contour lines represent the isopycnals and the increment among the isopycnals is 0.1 kg/m^3. The black bold line represents the MLD.

4. Discussion

4.1 Summary of Triaxus data quantity and quality

Triaxus data collected from 15 voyages of the *RV Investigator* were widely distributed around Australia, but mainly focussed in the east and south-east of Australia (Fig 5). The number of Triaxus tows during most of these voyages was less than or equal to 8, except the voyage IN2016V04 (17 tows), IN2017V04 (17 tows) and IN2018V05 (33 tows) (Table 1). The overall quality of Triaxus data was generally good in that the QC flag of each parameter was labelled good or excellent (Table 1). However, the data quality of all parameters in a tow was not the same due to the breakdown of individual sensors deployed on the Triaxus platform. Both optical backscatter and transmissivity measure the subsurface distribution of particulate and suspended matter, so the subsurface patterns of OBS and attenuation should generally be similar, which was generally observed (Figs 9, 12, 15 & 18). However, based on the QC flags and data

issues found within relevant Triaxus data processing reports, the transmissometer seemed more susceptible to abnormal observations of attenuation (Table 1). For example, (from the figure 12d) there was evidence for bad data quality from the voyage IN2016V04 tow 1 that was not captured by the QC flags. By this we mean the suspicious looking vertical 'band' of data near the start of the transect. Additionally, the voyage IN2018T01 tow 2 also had some suspicious attenuation data in the second half (Fig 9d), where the subsurface variation of OBS and attenuation did not significantly agree. There could be further issues within the data that users should be alerted to, and may require further quality assurance tests.

To further ensure the reliability of the Traixus data quality, in addition to the evaluation based on the QC flags, the surface chlorophyll concentration (detected in Triaxus data) can be compared with the satellite data. Here we used the 'shallowest' chlorophyll data obtained from the upper mixed layer by the Triaxus. Comparing the satellite Chl-a maps for the 4 tows (Figs 20a, 20b, 20c & 20d) with the Traixus chlorophyll showed that regions of high chlorophyll observed by the satellite corresponded with regions of high chlorophyll detected by the fluorometer on the Triaxus, as indicated by the red portion of the transects. This increases our confidence in the Triaxus chlorophyll data.

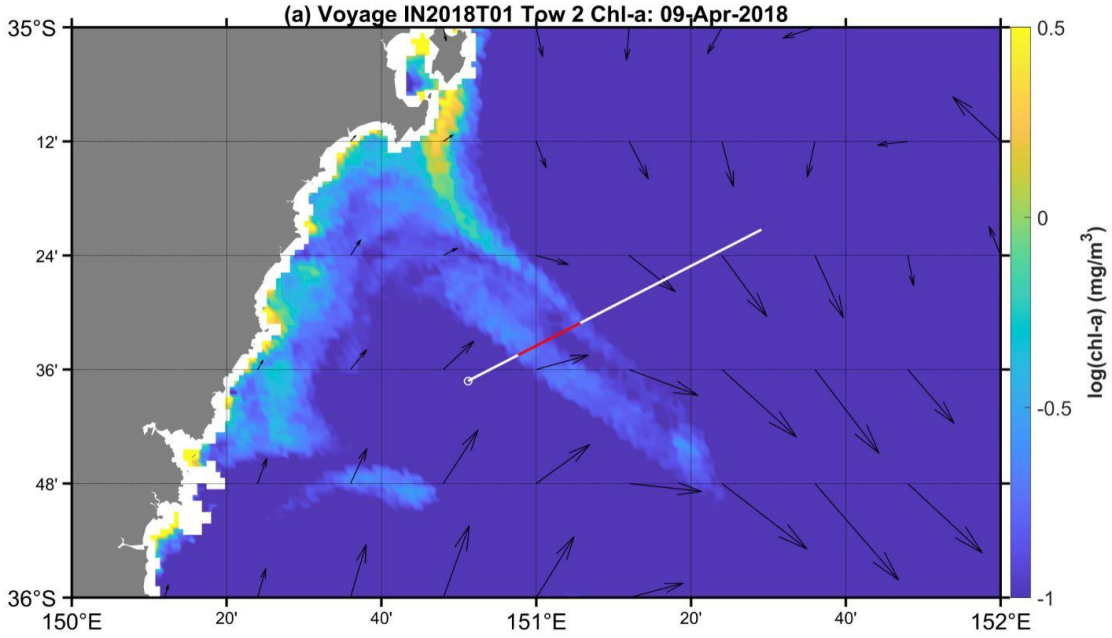

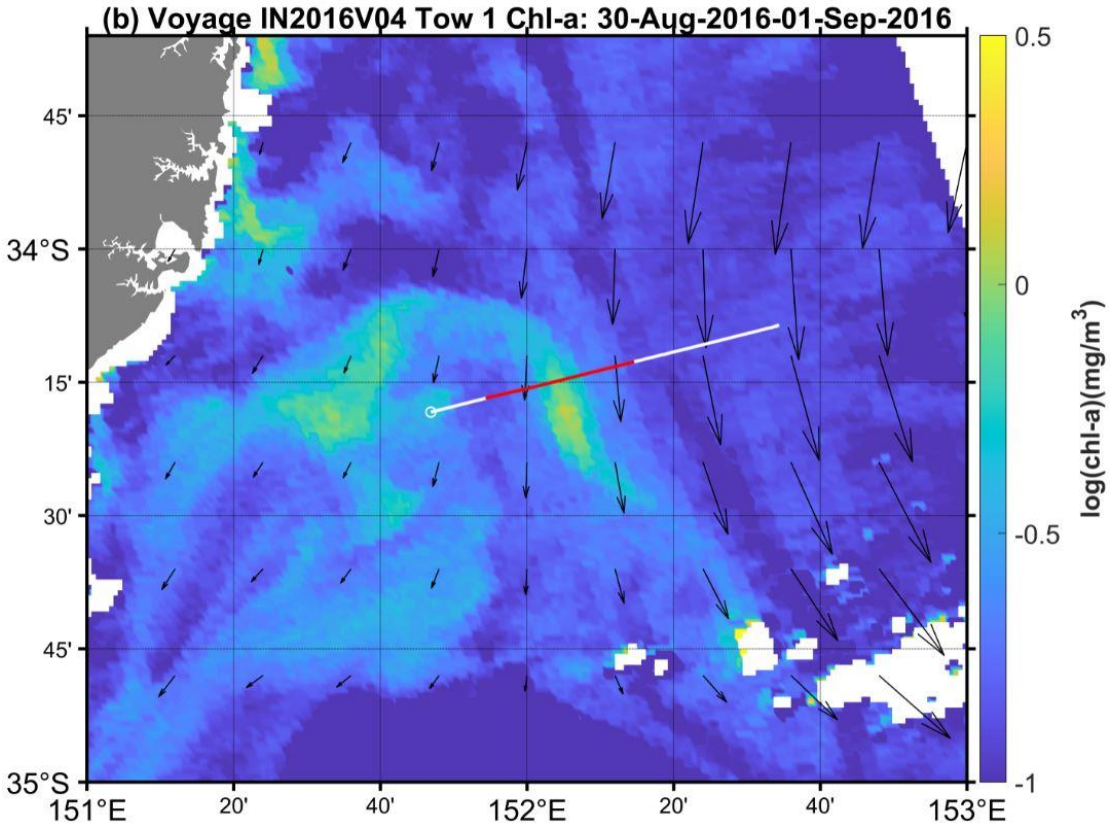
(b) Voyage IN2016V04 Tow 1 Chl-a: 30-Aug-2016-01-Sep-2016
45'
34°S
15'
30'
45'
35°S
151°E
20'
40'
152°E
20'
40'
153°E
0.5
0
-0.5
-1
log(chl-a)(mg/m3)

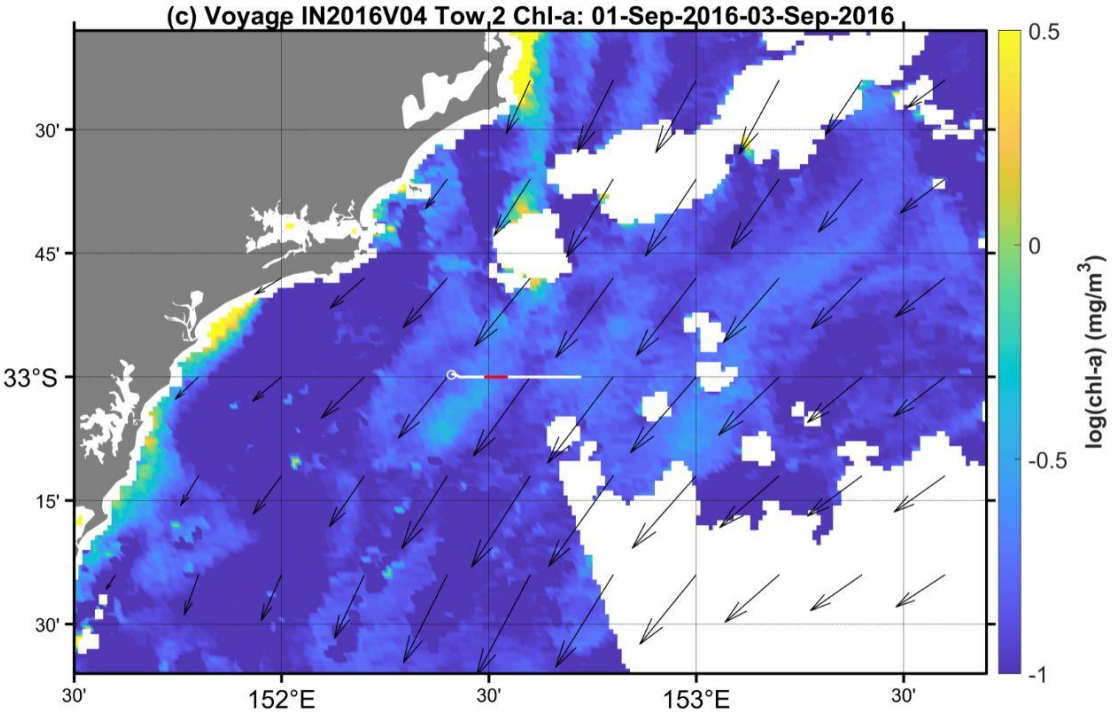
(c) Voyage IN2016V04 Tow 2 Chl-a: 01-Sep-2016-03-Sep-2016
30'
45'
33°S
15'
30'
30'
152°E
30'
153°E
30'
0.5
0
-0.5
-1
log(chl-a) (mg/m3)

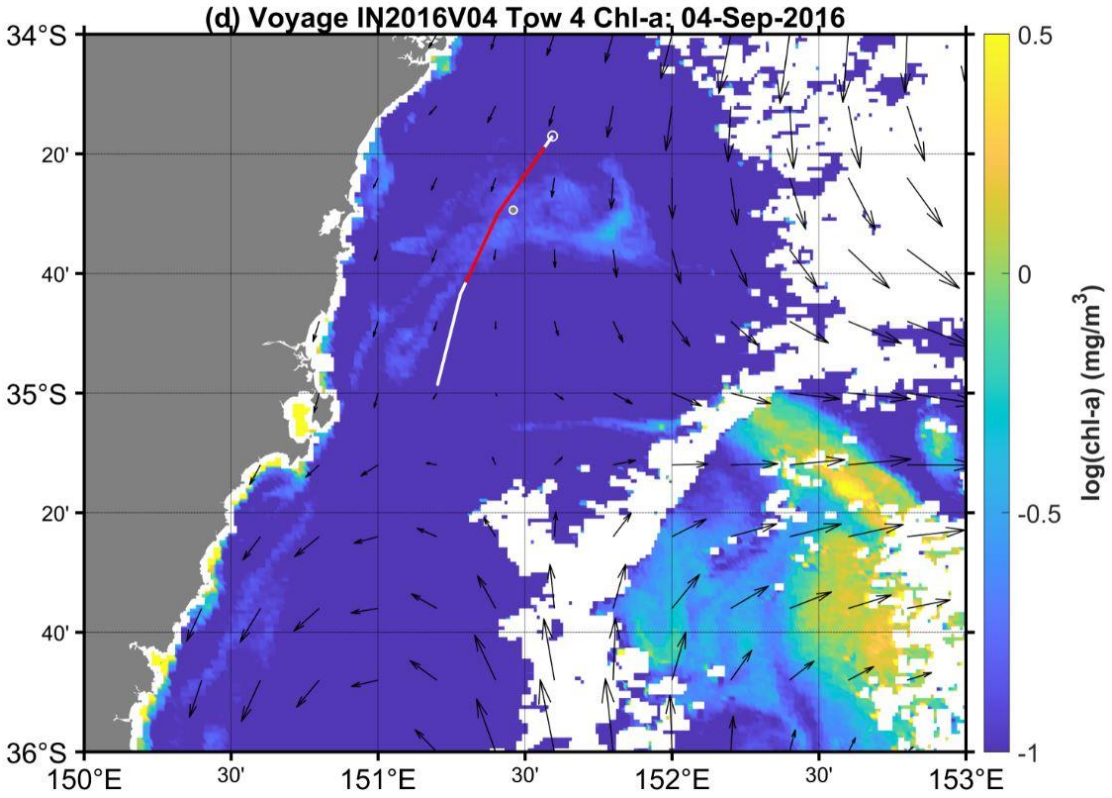

Figure 20. Chl-a Maps of study areas near the 4 tows including (a) the 2nd tow from the voyage IN2018T01 on the 9th of April 2018, (b) the 1st tow from voyage IN2016V04 on the 31th of August 2016, (c) the 2nd tow from voyage IN2016V04 on the 2nd of September 2016 and (d) the 4th tow from the voyage IN2016V04 on the 4th of September 2016, where background colours represent the logarithm of surface chlorophyll-a concentration. The blank space represents the area for which there was no Chl-a data. The direction and size of black arrows represent the direction and magnitude respectively, of surface geostrophic velocity. The white lines represent the track of these tows. The red lines represent the part of these transects where the subsurface high chlorophyll and OBS are observed in the Triaxus data. The Chl-a data on the 31th of August 2016 was derived by the Chl-a average of two adjacent dates including the 30th of August and the 1st of September 2016. The Chl-a data on the 2nd of September 2016 was derived by the Chl-a average of two adjacent dates including the 1st of September and the 3rd of September 2016.

For the voyage IN2018T01 tow 2, the chlorophyll concentration below the MLD (about

0.7-1.3 ug/L) was small compared to that seen above the MLD (about 0.1-0.6 ug/L) (Fig 9b), which basically matched the surface Chl-a concentration observed flowing through the area marked in red on the satellite Chl-a map (about 0.1-0.3 mg/m^3) (Fig 20a). Note, 1 ug/L is equal to 1 mg/m^3. For the voyage IN2016V04 tow 4, the chlorophyll above the MLD measured by Triaxus (0.6-0.9 ug/L) (Fig 18b), was higher than the concentration of surface Chl-a observed by the satellite (about 0.2-0.4 mg/m^3) (Fig 20d). This might be due to a discrepancy in the specific time data was observed by the satellite and Triaxus. Surface Chl-a passing through the transect increased with time with original surface chlorophyll sinking below the MLD. There was also another discrepancy in the two data sources whereby chlorophyll estimated by the Triaxus data was obtained by measuring the fluorescence, while Chl-a estimated by the satellite was derived by the multispectral measurement of sunlight from the reflection of the sea surface layer at multiple wavelengths (Cannizzaro & Carder 2006). Similarly, chlorophyll estimated by fluorescence has its own source of error, where the relationship between chlorophyll and fluorescence varies in different regions, depending on the dominant phytoplankton species and its pigment composition (Roesler et al. 2017).

For the voyage IN2016V04 tow 1, there was good agreement between Traixus near-surface chlorophyll (0.6 to 1.1 ug/L) (Fig 12b) and the satellite data (0.3-1.3 mg/m^3) (Fig 20b). For the voyage IN2016V04 tow 2, the Triaxus near-surface chlorophyll of 0.7 ug/L (Fig 15b) was obviously larger than the satellite Chl-a data (0.3-0.5 mg/m^3) (Fig 20c). Again, this small difference may reflect the difference in specific time between the satellite and Triaxus data. However, it was worth mentioning that there was another computational error for the two tows. Surface Chl-a was calculated by averaging data for up to 1 day before and after the date of each tow.

4.2 Characterisation of subsurface biomass features

For all the 4 tows, high subsurface chlorophyll was found to coexist alongside elevated OBS and attenuation. This indicated that the suspended particles observed in the upper ocean were living organisms with phytoplankton the primary component (Kawahata & Ohta 2000). Also included were non-chlorophyll matter such as decaying phytoplankton and products from this degradation. We defined the subsurface biomass peaks as regions with high concentration of chlorophyll (a proxy for phytoplankton) detected by the Triaxus data below the surface mixed layer, such as the maximum chlorophyll concentration observed below the MLD (about top 25-50 m) between 9 and 23 km (Fig 9b).

Combined observations of high chlorophyll, OBS and attenuation were a good measure of subsurface biomass, because fluorescence is not a perfect proxy for chlorophyll, which in turn is also not a perfect measure of biomass given phytoplankton cells contain more chlorophyll when there is less light, as a way of harvesting more light (Lichtenthaler et al. 1982). They can also produce less fluorescence when exposed to high light near the surface (Abbott, Richerson & Powell 1982). On the other hand, OBS and attenuation are not good measures of phytoplankton on their own, because non-photosynthetic material (such as sediment) can also absorb and scatter light (Morgan & Smith 1981).

A common feature for all the 4 tows was where subsurface biomass extended the deeper ocean as shown in the Figures 9b, 12b, 15b and 18b. Meanwhile, similar behaviours were also observed in OBS and attenuation; especially the OBS. The transmissometer used to detect attenuation of seawater seemed more susceptible to problems than the backscatter sensor. In this study, we identified the features involving subsurface biomass in accordance with high observed OBS.

4.3 Similar surface Chl-a histories and subsurface biomass sources

By analysing a time-series of maps of surface Chl-a in the regions of the tows, we determined that in all cases it looked like high chlorophyll had been recently advected into the area where the tow occurred, rather than having simply increased in the same place over time, or been constant for several days.

For the voyage IN2018T01 tow 2, the Shoalhaven coastal areas near the transect had high concentrations of chlorophyll (Chl-a) for the 7th of April. This was especially true for the northern region of the transect near the shoreline (Electronic Appendix III), when a nearby weak geostrophic current from the north was flowing southeast along the coastline and converging with a stronger geostrophic current flowing northeast from the south at the end of the transect, to form a strong southeast circulation flow southeast (after passing the transect). Here the subsurface horizontal velocity was dominantly zonal evidenced by the fact that the surface distribution pattern of the whole transect was closer to the zonal direction (Fig 20a).

Surface phytoplankton biomass in the northern coastal regions gradually became more abundant with time as observed by the increase in the concentration of Chl-a (Electronic Appendix III). Under the effect of surface currents, the surface phytoplankton was carried through the red portion of the transect (Fig 20a). Similarly, for the voyage IN2016V04 tow 1, 2 and 4, the historical maps of surface Chl-a also showed that the Chl-a from the nearshore area around the tows passed through the red portion of corresponding transects under the effect of geostrophic currents flowing from the north to the south (Figs 20b, c & d).

4.4 Process responsible for subsurface biomass peaks

Features observed in all the 4 tows showed subsurface biomass peaks entering the deeper ocean. This might be caused either by gravitational sinking, where particles and

aggregates in the upper ocean were transported downward by gravity, or by subduction, where organic matter was transported from the surface ocean to the mesopelagic by horizontal and vertical advection of surrounding water (Stukel et al. 2018). We have found evidence for both types of events in the Triaxus data as summarised in Table 2.

Tows	Oceanographic setting		Stratification	Bio-optical Properties					Likely mechanism
	Weak eddy	Front		OBS	Chl	Att	DO	AOU	
18_tow2	T	F	S	H	H	H	L	H	Gs
16_tow1	T	F	S	H	H	H	L	H	Gs
16_tow2	T	T	W	H	H	H	H	L	Sd
16_tow4	T	F	S	H	H	H	L	H	Gs

Table 2. Information associated with subsurface biomass peaks for the 4 tows. 'T' indicates there is weak eddy or front, and vice versa, using 'F'. W/S indicates the intensity of stratification (weak/strong) near the area where features occurred. The contents of backscatter (OBS), chlorophyll (Chl), attenuation (Atte), dissolved oxygen (DO) and apparent oxygen utilization (AOU) in the corresponding area are expressed in terms of high (H) and low (L), respectively. Likely mechanism is either gravitational sinking (Gs) or subduction (Sd), as the cause of features.

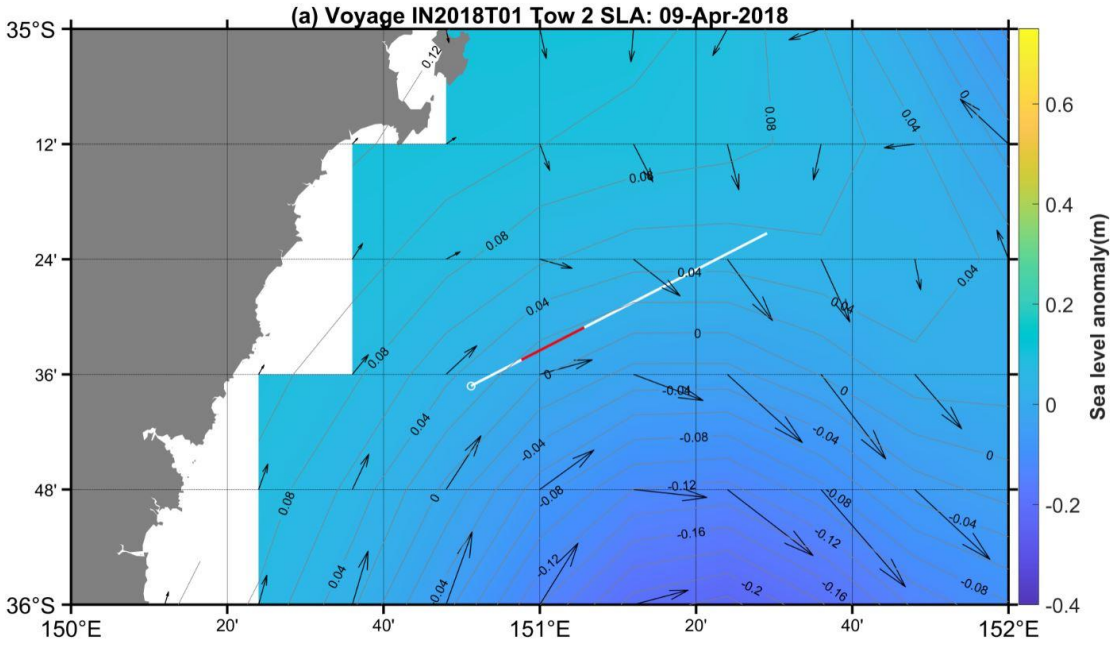

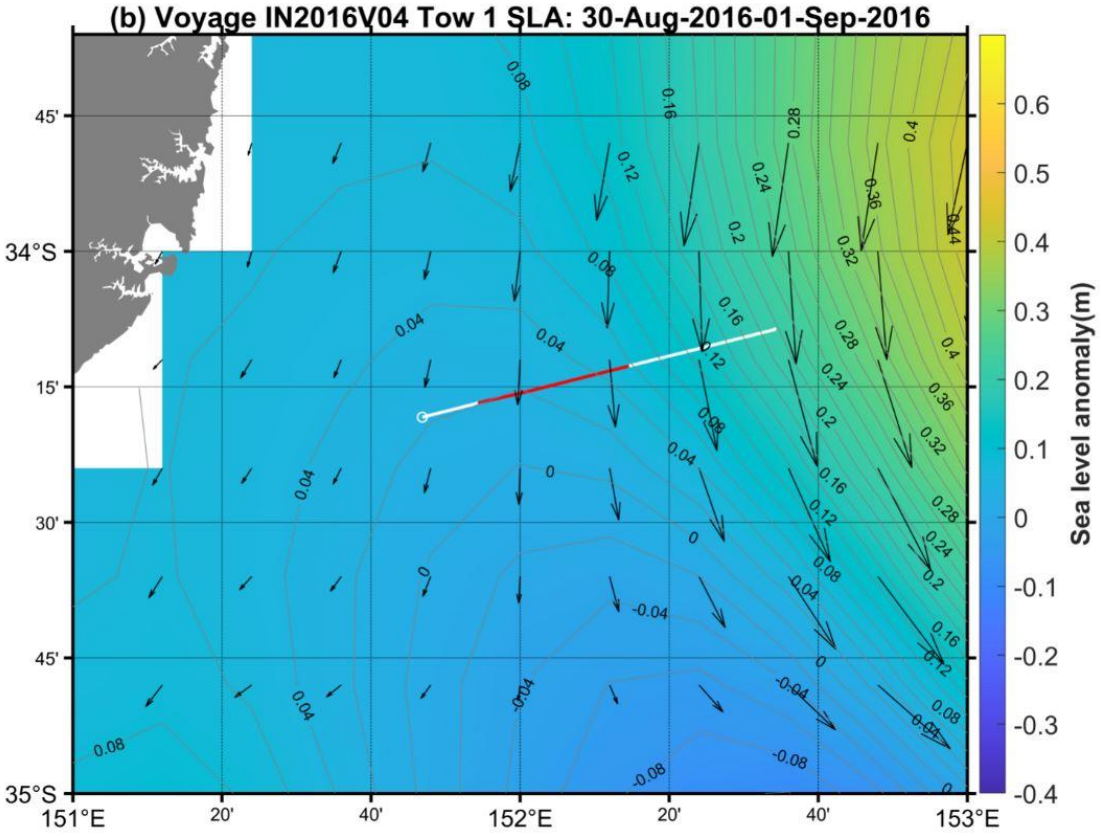
(b) Voyage IN2016V04 Tow 1 SLA: 30-Aug-2016-01-Sep-2016
45'
34°S
15'
30'
45'
35°S
151°E
20'
40'
152°E
20'
40'
153°E
Sea level anomaly(m)
0.6
0.5
0.4
0.3
0.2
0.1
0
-0.1
-0.2
-0.3
-0.4

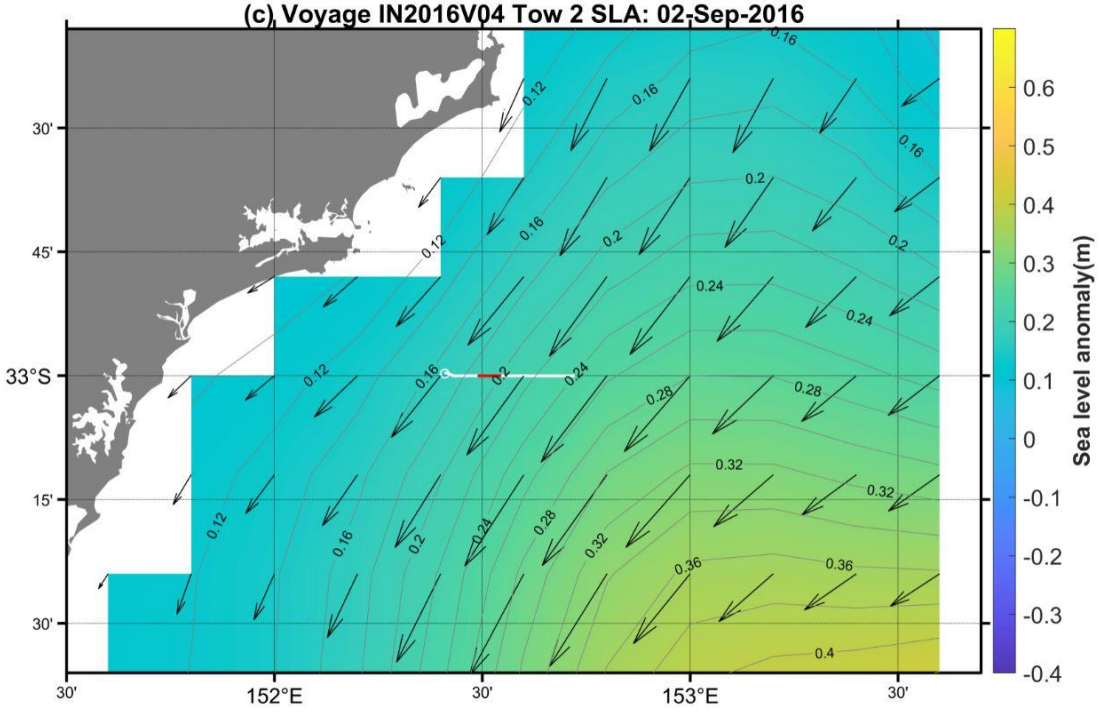
(c) Voyage IN2016V04 Tow 2 SLA: 02-Sep-2016
30'
45'
33°S
15'
30'
30'
152°E
30'
153°E
30'
Sea level anomaly(m)
0.6
0.5
0.4
0.3
0.2
0.1
0
-0.1
-0.2
-0.3
-0.4

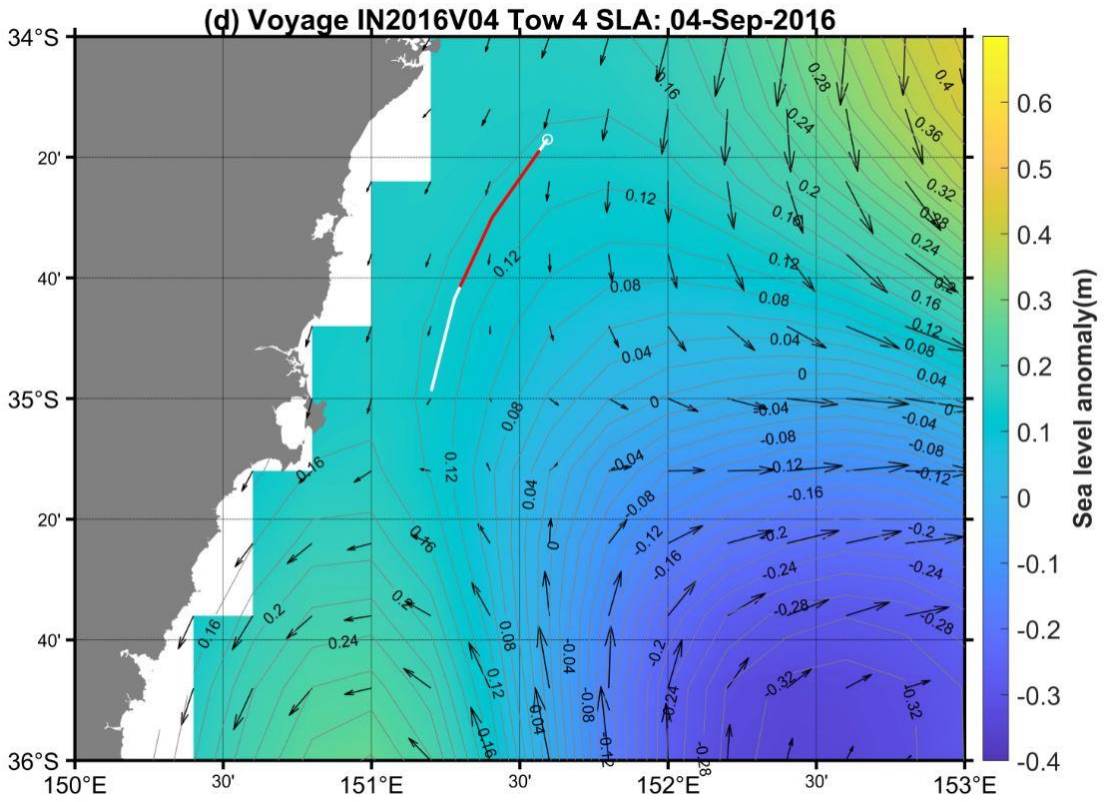

Figure 21. SLA maps of study areas near the 4 tows including (a) the 2nd tow from the voyage IN2018T01 on the 9th of April 2018, (b) the 1st tow from voyage IN2016V04 on the 31th of August 2016, (c) the 2nd tow from voyage IN2016V04 on the 2nd of September 2016 and (d) the 4th tow from the voyage IN2016V04 on the 4th of September 2016, where background colours represent the SLA and background contour lines represent the sea surface height. The increment in contour lines is 0.02 m. The blank space represents that there is no SLA data. The direction and size of black arrows respectively represent the direction and magnitude of surface geostrophic velocity. The white lines represent the track of these tows. The red lines represent the part of these transects where the subsurface biomass are observed in the Triaxus data. The SLA data on the 31th of August 2016 was derived by the SLA average of two adjacent date including the 30th of August and the 1st of September 2016.

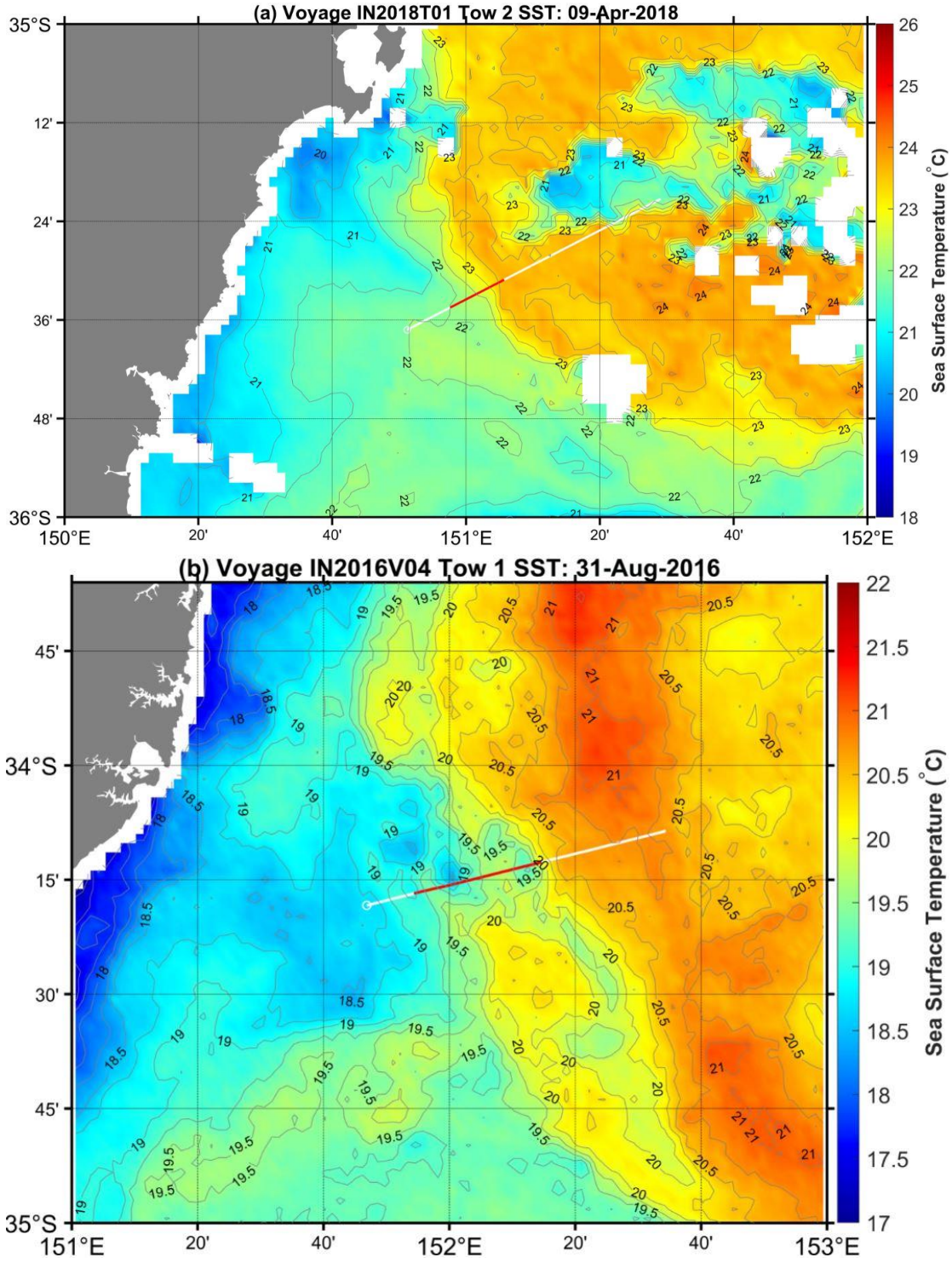
(a) Voyage IN2018T01 Tow 2 SST: 09-Apr-2018
35°S
12'
24'
36'
48'
36°S
150°E
20'
40'
151°E
20'
40'
152°E
Sea Surface Temperature (°C)
26
25
24
23
22
21
20
19
18
(b) Voyage IN2016V04 Tow 1 SST: 31-Aug-2016
45'
34°S
15'
30'
45'
35°S
151°E
20'
40'
152°E
20'
40'
153°E
Sea Surface Temperature (°C)
22
21.5
21
20.5
20
19.5
19
18.5
18
17.5
17

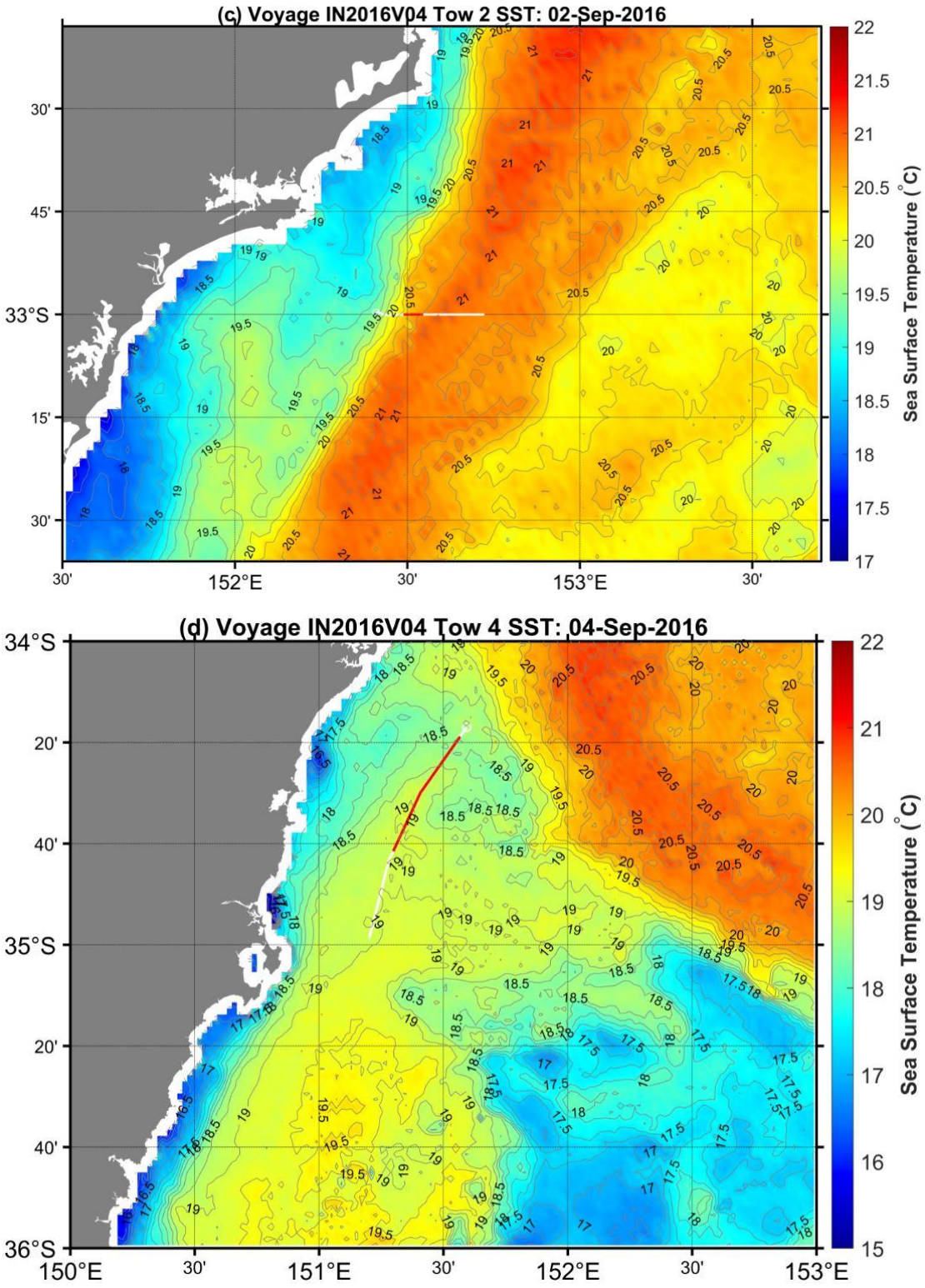

Figure 22. SST Maps of study areas near the 4 tows including (a) the 2nd tow from the voyage IN2018T01 on the 9th of April 2018, (b) the 1st tow from voyage IN2016V04 on the 31th of August 2016, (c) the 2nd tow from voyage IN2016V04 on the 2nd of September 2016 and (d) the 4th tow from the voyage IN2016V04 on the 4th of

September 2016, where background colours represent the SST and background contour lines represent the isotherms. The increments in contour lines for the voyage IN2018T01 and the voyage IN2016V04 respectively are 0.5℃ and 0.25 ℃. The blank space represents that there is no SST data. The white lines represent the track of these tows. The red lines represent the part of these transects where the subsurface biomass peaks are observed in the Triaxus data.

4.4.1 Suspected subduction events

During voyage IN2016V04 tow 2, a subsurface biomass feature was seen penetrating into deeper water below the MLD (Fig 15b), in the shape of a 'tongue' area. We considered this as highly likely to be a subduction event. Here, we found that the 'tongue' area was connected to the sea surface via a similar chlorophyll concentration (Fig 15b), with significant OBS peaks within the 'tongue' area (Fig 15a). Additionally, we found that the temperature, density and spiciness was nearly constant within the 'tongue' area (Figs 14a, d & e), and the stratification was weak here (Fig 14f). Weak stratification coupled with the instability of the MLD could contribute to a deep subduction of water masses (Erickson & Thompson 2018).

There was a significant front observed at the beginning of the transect with a strong temperature gradient (Fig 22b). This tow crossed the edge of the warm-core eddy 2 with strong geostrophic currents. Due to the eddies, strong geostrophic currents carried surface biomass from the surrounding area passing through the transect (Figs 20c & 21c). Meanwhile, there was very strong subsurface horizontal velocity westward along the transect (Fig 16a). Highly dynamic fronts could produce filaments that cross the front, differing in density from the surrounding environment (Mahadevan 2014). This would result in the generation of a subduction event because the density at the end of filament was similar to that of subsurface water, causing both water masses to mix (Omand et al. 2015). This was representative of the actual situation observed in the

Triaxus data where the spiciness was nearly constant in the ‘tongue’ area (Fig 14e), indicating surface water in the tongue area was connected to subsurface water with similar density.

Subsurface OBS peaks observed in the ‘tongue’ area were most likely due to subduction of surface water that carried high concentration chlorophyll from the surface layer (about top 50 m). Additionally, we found a similar ‘tongue’ area for the high DO and low AOU respectively and both were connected to the water above them with the same concentration (Figs 14c & 15e). It was also powerful evidence with which to prove the existence of the subduction. This was because the subduction of phytoplankton-rich surface waters would carry high dissolved oxygen from the surface layer and provide the necessary oxygen for the respiration of plankton (Mahadevan 2014). We therefore could confidently infer the ‘tongue’ area observed was due to the subduction of surface water.

4.4.2 Enhanced sinking without subduction

The subsurface biomass features observed in the voyage IN2018T01 tow 2 (transect 2) and the voyage IN2016V04 tow 1 (transect 1) and tow 4 (transect 4) (Fig 9b, 12b & 18b) were thought to be caused by gravitational sinking rather than subduction. Here, we named the regions where the subsurface OBS peaks were observed in the three transects as the ‘triangle’, ‘cone’ area and the ‘strip’ areas. These three tows did not show the same features involving the process of subsurface biomass peaks observed in the voyage IN2016V04 tow 2 including fronts, weak stratification, high DO and low AOU (Table 2).

A common feature that all the transects 1, 2 and 4 shared was that each passed through the edges of weak cold-core eddies with weak geostrophic currents (Figs 21a, b & d). There was also no explicit phenomenon indicating the existence of a surface front for

any of these three transects (Figs 22a, b & d). This basically negated the occurrence of a subduction event that could have been caused by the filament due to surface fronts.

The observed stratification favours gravitational sinking rather than subduction. For transect 2, near the area where subsurface biomass peaks occurred, the subsurface distribution of temperature, density and spiciness were well-structured (Figs 8a, d & e), indicating that the water masses were stable. Furthermore, stratification was stronger than the surrounding area because N^2 was obviously high (Fig 8f), indicating that vertical motion would be inhibited; vertical mixing rarely occurs even if there was strong horizontal velocity (Gubbins 2007). The above evidence further reduced the possibility that the occurrence of subsurface biomass in these areas was due to the subduction events, where the mixing of water masses would be present.

The disconnection between surface properties and subsurface properties provides more support for the "gravitational sinking" mechanism. With the subsurface horizontal velocity moving eastward along the zonal direction (Fig 10a), subsurface biomass occurring between 10 and 25 km moved along the isopycnals toward the end of the transect (Fig 9b). We found that the subsurface chlorophyll gradually decreased along the isopycnals when horizontal velocity decreased and the stratification became weaker. Meanwhile, we found that there was significantly high OBS between 20 and 40 km, in the 'triangle' area, but this was not connected to the peaks in the surface layer (about the top 60 m). Gravitational sinking is a good explanation for this 'disconnection' phenomenon whereby particles sunk due to their own gravity as stratification became weaker with sinking became gradually weaker and concentrated in the 'triangle' area as the water layer became denser in the vertical direction.

We found the 'triangle' area had low DO (Fig 8c) and high AOU (Fig 9e), in contrast to the subduction event. Furthermore, we found that chlorophyll was dominant in the

top half part of ‘triangle’ area and non-chlorophyll matter was dominant in the lower half part (Fig 9c). Both the dominance of chlorophyll-poor particles and the associated high AOU suggest the exported particles, primarily phytoplankton, had undergone some microbial degradation, which decreased chlorophyll fluorescence, and consumed oxygen (Mahadevan 2014). The above process was different with that occurring in the subduction event, which was associated with high DO and low AOU.

Similar explanations illustrate the mechanism of gravitational sinking for the ‘cone’ and ‘strip’ areas. First, subsurface biomass moved along the isopycnals due to subsurface horizonal velocity (Figs 12b & 18b). The subsurface horizontal velocities gradually became smaller, even reducing to zero in the two areas where the water masses were stable and the stratification was strong. This indicated that there was hardly horizontal and vertical motion. Thus gravitational sinking becomes responsible for the occurrence of these areas.. Similarly, we also found the low DO and high AOU in these two areas. All the above explanations strongly supported that the formation mechanism of these three areas was caused by the gravitational sinking rather than the subduction events.

It is worth noting that there was the filamentous subsidence of dissolved oxygen observed in these areas (Figs 8c, 11c & 17c). Combined with the amount of non-chlorophyll matter (Figs 9c, 12c & 18c), we found that the abnormally little high DO found as a filamentous pattern in the three areas tended to accompany higher levels of chlorophyll than OBS, which indicated that there were more phytoplankton with more chlorophyll to adapt the condition of low light, so that they produced oxygen dissolved in the seawater through their photosynthesis. Also of note in transect 4, is the region of very deep MLD at the end of the transect, where there was chlorophyll but little OBS (Fig 18c), which was because the phytoplankton have a high ratio of chlorophyll to biomass, as an adaptation to low light conditions. Unlike the phytoplankton growing under high light conditions, the phytoplankton that adapted to low light intensity would

develop chloroplasts containing more chlorophyll as a result of normal growth induced by their photosensitive pigments (Lichtenthaler et al. 1982).

4.5 Relationship between CDOM and AOU

In all 4 tows the subsurface distribution pattern of CDOM was very similar to that of AOU (Figs 9, 12, 15 & 18). From the figure 23, we can see that the subsurface variation of CDOM with depth in the upper layer (about top 200 m), although it looked noisy, was positively correlated with that of AOU. This finding is consistent with the conclusion of Nelson et al. (2010) that the distribution of CDOM was positively correlated with AOU in the surface layer (about top 1 km) of the Pacific, indicating that CDOM was dominantly a by-product of oxidized organic matter from sinking particles.

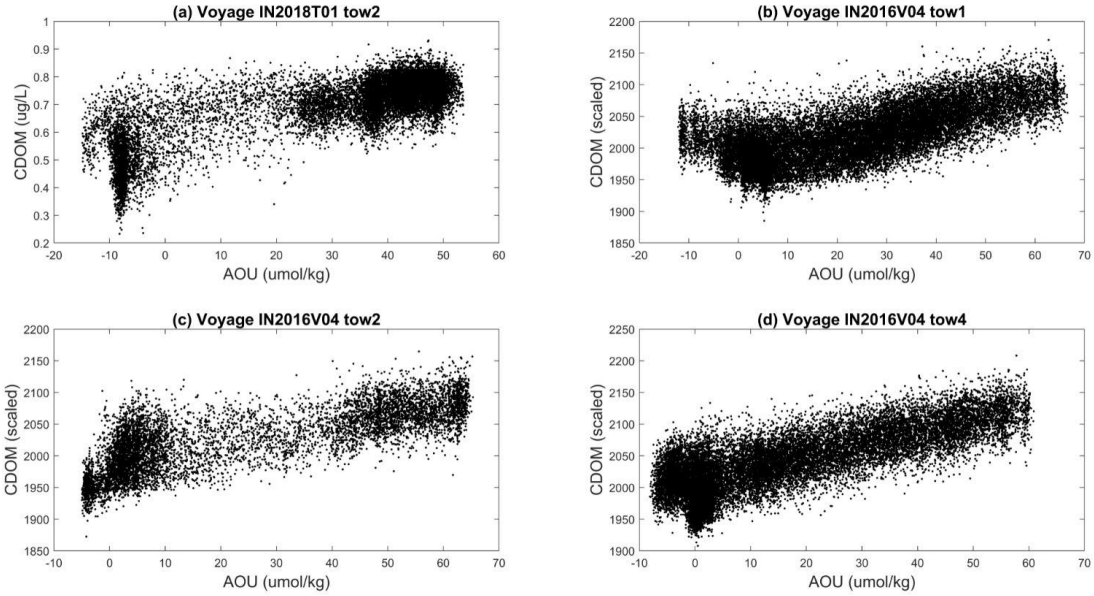

Figure 23. Scatter plot showing the relationship between AOU and CDOM from the 4 tows in the EAC region.

5. Conclusions and implications for future work

We evaluated the quantity and quality of Triaxus data collected by *RV Investigator* over the last five years. Triaxus has been towed thousands of kilometers around Australia on 15 voyages and 127 tows. Triaxus is an oceanographic platform deployed with diverse

sensors to collect biogeochemical information, so we have to make sure that each sensor works to produce good quality data. To better enable Triaxus data to accurately estimate oceanographic information, the data quality needs to be further evaluated in addition to the current QC testing. We hope that future work will establish a comprehensive assessment system for the Triaxus data, which will benefit Triaxus data applications in exploring biogeochemical processes.

In this study, by combining fine-scale biogeochemical and physical oceanographic information, Triaxus data has been used to identify the mechanism responsible for the features observed where biomass was observed entering the deep sea in the EAC. Using Triaxus data we detected 1 example of a subduction event, and 3 examples of likely gravitational sinking events. The dominant factors driving these processes are eddies and fronts, which have vertical motions as well as strong horizontal motions. We hope the future work can further deepen the research in this field, such as by estimating vertical velocity from density and horizontal velocity. In addition, there are still many similar features that need further research to explore in the future work. This study only explores the relationship between particulate matter and backscatter, thus indirectly reflecting the fate of POC export. The future work can further investigate the relationship between POC and backscatter in the Australian region. Overall, Triaxus offers great potential for mapping and understanding fine scale features related to carbon export in the oceans around Australia.

6. References

Abbott, MR, Richerson, PJ & Powell, TM 1982, 'In situ response of phytoplankton fluorescence to rapid variations in light 1', *Limnology and Oceanography*, vol. 27, no. 2, pp. 218-225.

Badin, G, Williams, R, Holt, J & Fernand, L 2009, 'Are mesoscale eddies in shelf seas formed by baroclinic instability of tidal fronts?', *Journal of Geophysical Research: Oceans*, vol. 114, no. C10.

Bakun, A 2006, 'Fronts and eddies as key structures in the habitat of marine fish larvae: opportunity,

adaptive response and competitive advantage', *Scientia Marina*, vol. 70, no. S2, pp. 105-122.

Boyd, PW, Claustre, H, Levy, M, Siegel, DA & Weber, T 2019, 'Multi-faceted particle pumps drive carbon sequestration in the ocean', *Nature*, vol. 568, no. 7752, p. 327.

Briggs, N, Perry, MJ, Cetinić, I, Lee, C, D'Asaro, E, Gray, AM & Rehm, E 2011, 'High-resolution observations of aggregate flux during a sub-polar North Atlantic spring bloom', *Deep Sea Research Part I: Oceanographic Research Papers*, vol. 58, no. 10, pp. 1031-1039.

Bushnell, M, Kinkade, C & Worthington, H 2017, 'Manual for real-time quality control of ocean optics data: a guide to quality control and quality assurance of coastal and oceanic optics observations'.

Cannizzaro, JP & Carder, KL 2006, 'Estimating chlorophyll a concentrations from remote-sensing reflectance in optically shallow waters', *Remote Sensing of Environment*, vol. 101, no. 1, pp. 13-24.

Cetinić, I, Perry, MJ, Briggs, NT, Kallin, E, D'Asaro, EA & Lee, CM 2012, 'Particulate organic carbon and inherent optical properties during 2008 North Atlantic Bloom Experiment', *Journal of Geophysical Research: Oceans*, vol. 117, no. C6.

Chisholm, SW 2000, 'Oceanography: stirring times in the Southern Ocean', *Nature*, vol. 407, no. 6805, p. 685.

Commission, IO 2015, 'The International thermodynamic equation of seawater–2010: calculation and use of thermodynamic properties.[includes corrections up to 31st October 2015]'.

Cromwell, T & Reid Jr, JL 1956, 'A Study of Oceanic Fronts 1', *Tellus*, vol. 8, no. 1, pp. 94-101.

de Boyer Montégut, C, Madec, G, Fischer, AS, Lazar, A & Iudicone, D 2004, 'Mixed layer depth over the global ocean: An examination of profile data and a profile-based climatology', *Journal of Geophysical Research: Oceans*, vol. 109, no. C12.

Dohan, K & Sutherland, B 2003, 'Internal waves generated from a turbulent mixed region', *Physics of Fluids*, vol. 15, no. 2, pp. 488-498.

Erickson, ZK & Thompson, AF 2018, 'The seasonality of physically driven export at submesoscales in the northeast Atlantic Ocean', *Global Biogeochemical Cycles*, vol. 32, no. 8, pp. 1144-1162.

Flament, P 2002, 'A state variable for characterizing water masses and their diffusive stability: spiciness', *Progress in Oceanography*, vol. 54, no. 1-4, pp. 493-501.

Frouin, R & Murakami, H 2007, 'Estimating photosynthetically available radiation at the ocean surface from ADEOS-II global imager data', *Journal of oceanography*, vol. 63, no. 3, pp. 493-503.

Gubbins, D 2007, 'Geomagnetic constraints on stratification at the top of Earth's core', *Earth, planets and space*, vol. 59, no. 7, pp. 661-664.

Guidi, L, Calil, PH, Duhamel, S, Björkman, KM, Doney, SC, Jackson, GA, Li, B, Church, MJ, Tozzi, S & Kolber, ZS 2012, 'Does eddy-eddy interaction control surface phytoplankton distribution and carbon export in the North Pacific Subtropical Gyre?', *Journal of Geophysical Research: Biogeosciences*, vol. 117, no. G2.

Hansen, LF & Hansen, HJ 2003, 'Triaxus: A 3D undulating towed underwater vehicle', *International Ocean Systems*, vol. 7, no. 2, pp. 10-13.

Hazeleger, W & Drijfhout, S 2000, 'Eddy subduction in a model of the subtropical gyre', *Journal of physical oceanography*, vol. 30, no. 4, pp. 677-695.

Honjo, S, Dymond, J, Prell, W & Ittekkot, V 1999, 'Monsoon-controlled export fluxes to the interior of the Arabian Sea', *Deep Sea Research Part II: Topical Studies in Oceanography*, vol. 46, no. 8-9, pp. 1859-1902.

Johnson, KS & Coletti, LJ 2002, 'In situ ultraviolet spectrophotometry for high resolution and long-term monitoring of nitrate, bromide and bisulfide in the ocean', *Deep Sea Research Part I: Oceanographic Research Papers*, vol. 49, no. 7, pp. 1291-1305.

Johnson, KS, Plant, JN, Coletti, LJ, Jannasch, HW, Sakamoto, CM, Riser, SC, Swift, DD, Williams, NL, Boss, E, Haëntjens, N, Talley, LD & Sarmiento, JL 2017, 'Biogeochemical sensor performance in the SOCCOM profiling float array', *Journal of Geophysical Research: Oceans*, vol. 122, no. 8, pp. 6416-6436.

Kawahata, H & Ohta, H 2000, 'Sinking and suspended particles in the South-west Pacific', *Marine and freshwater research*, vol. 51, no. 2, pp. 113-126.

Lalli, C & Parsons, TR 1997, *Biological oceanography: an introduction*, Elsevier.

Lichtenthaler, H, Kuhn, G, Prenzel, U, Buschmann, C & Meier, D 1982, 'Adaptation of chloroplast-ultrastructure and of chlorophyll-protein levels to high-light and low-light growth conditions', *Zeitschrift für Naturforschung C*, vol. 37, no. 5-6, pp. 464-475.

Mahadevan, A 2014, 'Ocean science: Eddy effects on biogeochemistry', *Nature*, vol. 506, no. 7487, pp. 168-169.

Marshall, D 1997, 'Subduction of water masses in an eddying ocean', *Journal of Marine Research*, vol. 55, no. 2, pp. 201-222.

Martini, M, Butman, B & Mickelson, MJ 2007, 'Long-term performance of Aanderaa optodes and Sea-Bird SBE-43 dissolved-oxygen sensors bottom mounted at 32 m in Massachusetts Bay', *Journal of Atmospheric and Oceanic Technology*, vol. 24, no. 11, pp. 1924-1935.

McDougall, T, Jackett, D, Millero, FJ, Pawlowicz, R & Barker, P 2012, 'A global algorithm for estimating Absolute Salinity', *Ocean Science*, vol. 8, no. 6.

McDougall, TJ & Krzysik, OA 2015, 'Spiciness', *Journal of Marine Research*, vol. 73, no. 5, pp. 141-152.

McGillicuddy, DJ, Anderson, LA, Bates, NR, Bibby, T, Buesseler, KO, Carlson, CA, Davis, CS, Ewart, C, Falkowski, PG & Goldthwait, SA 2007, 'Eddy/wind interactions stimulate extraordinary mid-ocean plankton blooms', *Science*, vol. 316, no. 5827, pp. 1021-1026.

Morgan, D & Smith, H 1981, 'Non-photosynthetic responses to light quality', in *Physiological plant ecology I*, Springer, pp. 109-134.

Nelson, NB, Siegel, DA, Carlson, CA & Swan, CM 2010, 'Tracing global biogeochemical cycles and meridional overturning circulation using chromophoric dissolved organic matter', *Geophysical Research Letters*, vol. 37, no. 3.

Neuer, S, Iversen, M & Fischer, G 2014, 'The Ocean's Biological Carbon Pump as Part of the Global Carbon Cycle', *Limnology and Oceanography e-Lectures*, vol. 4, no. 4, pp. 1-51.

Newton, PP, Lampitt, RS, Jickells, TD, King, P & Boutle, C 1994, 'Temporal and spatial variability of biogenic particles fluxes during the JGOFS northeast Atlantic process studies at 47° N, 20° W', *Deep Sea Research Part I: Oceanographic Research Papers*, vol. 41, no. 11-12, pp. 1617-1642.

Omand, MM, D'Asaro, EA, Lee, CM, Perry, MJ, Briggs, N, Cetinić, I & Mahadevan, A 2015, 'Eddy-driven subduction exports particulate organic carbon from the spring bloom', *Science*, vol. 348, no. 6231, pp. 222-225.

Pender, L 2000, 'Data Quality Control Flags', *Availabe online at http://www. marine. csiro. au/datacentre/ext_docs/DataQualityControlFlags. pdf*.

Resplandy, L, Lévy, M & McGillicuddy Jr, DJ 2018, 'Effects of eddy-driven subduction on ocean biological carbon pump', *Global Biogeochemical Cycles*.

Roesler, C, Uitz, J, Claustre, H, Boss, E, Xing, X, Organelli, E, Briggs, N, Bricaud, A, Schmechtig, C & Poteau, A 2017, 'Recommendations for obtaining unbiased chlorophyll estimates from in situ chlorophyll fluorometers: A global analysis of WET Labs ECO sensors', *Limnology and Oceanography: Methods*,

vol. 15, no. 6, pp. 572-585.

Rubenstein, DM & Roberts, GO 1986, 'Scattering of inertial waves by an ocean front', *Journal of physical oceanography*, vol. 16, no. 1, pp. 121-131.

Schultes, S & Lopes, RM 2009, 'Laser Optical Plankton Counter and Zooscan intercomparison in tropical and subtropical marine ecosystems', *Limnology and Oceanography: Methods*, vol. 7, no. 11, pp. 771-784.

Sokolov, S & Rintoul, SR 2002, 'Structure of Southern Ocean fronts at 140 E', *Journal of Marine Systems*, vol. 37, no. 1-3, pp. 151-184.

Spall, MA 1995, 'Frontogenesis, subduction, and cross-front exchange at upper ocean fronts', *Journal of Geophysical Research: Oceans*, vol. 100, no. C2, pp. 2543-2557.

Stukel, MR, Aluwihare, LI, Barbeau, KA, Chekalyuk, AM, Goericke, R, Miller, AJ, Ohman, MD, Ruacho, A, Song, H & Stephens, BM 2017, 'Mesoscale ocean fronts enhance carbon export due to gravitational sinking and subduction', *Proceedings of the National Academy of Sciences*, vol. 114, no. 6, pp. 1252-1257.

Stukel, MR, Song, H, Goericke, R & Miller, AJ 2018, 'The role of subduction and gravitational sinking in particle export, carbon sequestration, and the remineralization length scale in the California Current Ecosystem', *Limnology and Oceanography*, vol. 63, no. 1, pp. 363-383.

Sweeney, EN 2001, 'Monthly variability in upper ocean biogeochemistry due to mesoscale eddy activity in the Saragasso Sea', Massachusetts Institute of Technology.

Thomson, RE & Emery, WJ 2014, *Data analysis methods in physical oceanography*, Newnes.

Turner, J 1981, 'Small-scale mixing-processes', *Evolution of physical oceanography*, pp. 236-262.

Vallis, G 2006, *Atmospheric and oceanic fluid dynamics: fundamentals and large-scale circulation–Cambridge University Press*, Cambridge.

Xu, L, Xie, SP, McClean, JL, Liu, Q & Sasaki, H 2014, 'Mesoscale eddy effects on the subduction of North Pacific mode waters', *Journal of Geophysical Research: Oceans*, vol. 119, no. 8, pp. 4867-4886.

7. Appendices

Here are links to the three electronic appendices:

Electronic Appendix I:

(https://metadata.imas.utas.edu.au/geonetwork/srv/eng/metadata.show?uuid=c9e2de6

1-9aad-4755-b8cf-8b96d32d35fe);

Electronic Appendix II:

(https://metadata.imas.utas.edu.au/geonetwork/srv/eng/metadata.show?uuid=c9e2de61-9aad-4755-b8cf-8b96d32d35fe);

Electronic Appendix III:

(https://metadata.imas.utas.edu.au/geonetwork/srv/eng/metadata.show?uuid=c9e2de61-9aad-4755-b8cf-8b96d32d35fe).

These electronic appendices will be published on the IMAS Data Portal in the future.